doi:10.26443/seismica.v5i1.1713

Paleoseismic trenching on slip-partitioned surface ruptures associated with the 2016 Kumamoto earthquake

Daisuke Ishimura * [1], **Naoya O. Takahashi** [2], **Hiroyuki Tsutsumi**[3], **Shin'ichi Homma**[4], **Sakae Mukoyama**[4], **Toshihiko Ichihara**[5]

[1]Department of Earth Sciences, Chiba University, 1-33 Yayoi-cho, Inage-ku, Chiba 263-8522, Japan, [2]Department of Earth Science, Tohoku University, 6-3 Aoba, Aoba-ku, Sendai 980-8578, Japan, [3]Department of Environmental Systems Science, Doshisha University, 1-3 Tataramiyakodani, Kyotanabe, Kyoto 610-0394, Japan, [4]Department of Research & Development of Kokusai Kogyo Co., Ltd., 2-24-1 Harumi-cho, Fuchu, Tokyo 183-0057, Japan, [5]Faculty of Social and Cultural Studies, Kyusyu University, 744 Motooka, Nishi-ku, Fukuoka 819-0395, Japan

Author contributions: *Conceptualization*: D. Ishimura. *Data Curation*: N. O. Takahashi, S. Homma, S. Mukoyama. *Formal Analysis*: D. Ishimura, S. Homma, S. Mukoyama. *Funding Acquisition*: D. Ishimura. *Investigation*: D. Ishimura, N. O. Takahashi, H. Tsutsumi, T. Ichihara. *Methodology*: D. Ishimura, S. Homma, S. Mukoyama. *Project Administration*: D. Ishimura. *Resources*: D. Ishimura. *Software*: S. Homma, S. Mukoyama. *Supervision*: H. Tsutsumi. *Validation*: D. Ishimura. *Visualization*: D. Ishimura, N. O. Takahashi. *Writing – original draft*: D. Ishimura. *Writing – review & editing*: N. O. Takahashi, H. Tsutsumi, S. Homma, S. Mukoyama.

Abstract In large earthquakes, surface ruptures of secondary faults may appear in addition to the primary fault rupture, such as in the 2016 Kumamoto earthquake. Although the displacement of such distributed surface ruptures is small, information on their paleo activities may provide clues for evaluating displacement hazard and whether they can offer a paleoseismic history of the primary fault. We conducted lidar differencing analysis and trench excavation on the Idenokuchi fault, which was activated simultaneously with the primary Futagawa fault during the 2016 Kumamoto earthquake. First, we clarify the 3D displacement field by lidar differencing and quantify how slip partitioning occurred on both faults. We find that deep oblique slip is completely split into horizontal and vertical components at the ground surface and infer that the Idenokuchi fault is structurally connected to the Futagawa fault. Then, we excavate a trench on a subparallel surface rupture of the Idenokuchi fault and identify at least six (and potentially up to eight) faulting events since 15 ka. Combined with the results of other paleoseismic trenches, our findings on the Idenokuchi fault indirectly suggest that the Futagawa fault has ruptured relatively periodically. We conclude that subsidiary and secondary surface ruptures appeared in the last few events, as was the case during the 2016 event.

Non-technical summary We conducted a study on the Idenokuchi fault, which moved together with the main Futagawa fault during the 2016 Kumamoto earthquake, Japan. By comparing the topography before and after the earthquake, and by digging a trench, we were able to understand how the fault moved during the 2016 earthquake and during the prehistoric earthquakes. Our findings indicate that the oblique displacement on the fault at depth is split into horizontal and vertical movements at the surface. This suggests that the Idenokuchi fault merges with the Futagawa fault at depth. By digging a trench on the Idenokuchi fault, we found evidence for at least six (and potentially up to eight) past earthquakes over the last 15,000 years. The recurrence interval revealed on the Idenokuchi fault indirectly indicates that the Futagawa fault has ruptured at somewhat regular intervals. These findings contribute to a better understanding of earthquake hazards.

要旨 (日本語) 2016年熊本地震のような大地震の際に主断層周辺に加えて二次的な断層が出現することがある．そのような断層の変位は小さいが，その過去の活動の情報は変位ハザードリスクや主断層の活動履歴の復元に有用な手がかりとなる．そこで我々はlidar差分解析とトレンチ掘削調査を2016年熊本地震の際に布田川断層と同時に活動しスリップパーティションが生じたとされた出ノ口断層で実施した．まず，lidar差分により3次元変位場を求め，スリップパーティションが両断層でどのように生じたかを定量的に議論した．その結果，深部の斜めすべりが地表では完全に水平成分と鉛直成分に分割されたことが明らかとなり，出ノ口断層は構造的に布田川断層と地下でつながっていることが推定された．また，出ノ口断層に並走する断層上でトレンチ掘削した結果，15 ka以降に少なくとも6回，最大8回のイベントを推定した．他のトレンチ掘削の結果を合わせて考えると，我々の結果は布田川断層が比較的周期的に活動したことと，最近数回のイベントでは2016年同様に多くの断層が地表に出現したことを示唆する．

Production Editor:
Andrea Llenos
Handling Editor:
Randolph Williams
Copy & Layout Editor:
Ethan Williams

Signed reviewer(s):
Rich Koehler

Received:
August 5, 2025
Accepted:
January 12, 2026
Published:
April 6, 2026

*Corresponding author: ishimura@chiba-u.jp

1 Introduction

Recent developments in remote sensing technology (e.g., SAR and optical correlation) have enabled the capture of ground surface displacement associated with earthquakes with high resolution and precision, including the distribution and amount of displacement. As a result, it has become clear that the distribution of coseismic surface ruptures is complex when viewed in detail, and in some cases, ruptures are distributed over extensive areas (e.g., the 2016 Kumamoto earthquake (e.g., Fujiwara et al., 2016; Kumahara et al., 2022), the 2016 Kaikoura earthquake (e.g., Hamling et al., 2017; Litchfield et al., 2018), and the 2019 Ridgecrest earthquake (e.g., Barnhart et al., 2019; Xu et al., 2020)). Such complex ruptures have involved contemporaneous slip on the primary faults and other related faults, which are variably referred to as secondary, subsidiary, sympathetic, and distributed faults (e.g., Nurminen et al., 2020, 2022). Understanding the history and distribution of complex ruptures is important for assessing displacement hazards; however, few studies have evaluated the relative synchronicity of past ruptures along primary faults and their associated nearby faults.

The epicentral area of the Mw7.0 2016 Kumamoto earthquake provides a rare opportunity to study such co-rupturing events. InSAR analyses and field surveys have shown that the surface ruptures were widely distributed around the main (primary) fault of the 2016 Kumamoto earthquake (Fujiwara et al., 2016). Detailed field reconnaissance studies confirmed surface displacements and/or deformation at discontinuities observed in the InSAR data (Goto et al., 2017; Ishimura et al., 2017; Okamura et al., 2018; Sato et al., 2021). In addition to the ruptures along the primary Futagawa and Hinagu faults, surface displacements were observed along the Idenokuchi and Miyaji faults (Fig. 1). The Idenokuchi fault extends for approximately 10 km parallel to and within 2 km southeast of the Futagawa fault. Along this parallel section of the rupture, right-lateral displacement occurred on the Futagawa fault and vertical displacement occurred on the Idenokuchi fault, from which Toda et al. (2016) inferred that the slip was partitioned between the two faults. This suggests that the Futagawa and Idenokuchi faults merge at depth and are structurally connected. The Miyaji faults (Fig. 1; Ishimura et al., 2017) have the same strike and displacement sense as the Futagawa fault. However, the fault model based on the InSAR analysis (Fukushima and Ishimura, 2020) has revealed that the Miyaji faults are not connected to the Futagawa fault, suggesting that the 2016 surface ruptures on the Miyaji faults were triggered slip. These observations indicate that various mechanisms may have contributed to the surface ruptures around the Futagawa fault during the 2016 Kumamoto earthquake.

In addition to field measurements of fault displacements (Shirahama et al., 2016; Okamura et al., 2018; Kumahara et al., 2022), the three-dimensional deformation caused by the 2016 event has been revealed by InSAR and differential light detection and ranging (lidar) analyses (Moya et al., 2017; Scott et al., 2018; He et al., 2019; Himematsu and Furuya, 2020; Aoyagi et al., 2021; Muroi et al., 2024). In particular, lidar differencing provides higher resolution and more accurate displacement information in areas with larger displacements than InSAR analysis. These types of analyses have been conducted along some parts of the 2016 rupture (Scott et al., 2018; Aoyagi et al., 2021; Muroi et al., 2024), revealing the details of three-dimensional deformation.

After the 2016 Kumamoto earthquake, more than 10 paleoseismic trenches were excavated on the Futagawa and surrounding faults (Fig. 1). A paleoseismic survey (Miyaji trench in Fig. 1) conducted on the Miyaji faults revealed that the fault moved about 2,000 years ago before the 2016 event, which is consistent with the age range of the penultimate event of the Futagawa fault estimated by paleoseismic trenches (Ishimura et al., 2021). Furthermore, the vertical displacement in the penultimate event at the Miyaji trench was 10–20 cm, similar to the 2016 event, suggesting that the slip on the Miyaji faults has been repeatedly triggered by the slip on the Futagawa fault in the past. Other trenching survey on short surface ruptures of the 2016 event at the northwest of the Aso caldera also indicated activity preceding the 2016 event (Sato et al., 2021), suggesting the possibility of repeated synchronous ruptures. The interpretation of these trenches benefited from site conditions characterized by rapid sedimentation rates and multiple thin tephra layers (downwind of the Aso volcano), which enabled the identification of displacements as small as approximately 15 cm (Ishimura et al., 2021). The success of these efforts prompted us to search for sites along other faults near the Futagawa fault to examine the timing of events and potential contemporaneous rupture with the Futagawa fault.

In this study, we use lidar-based digital terrain models (DTMs) before and after the earthquake to calculate the three-dimensional displacement fields across the Futagawa and Idenokuchi faults, examining the amount of slip partitioning during the 2016 Kumamoto earthquake. Although Scott et al. (2018), Aoyagi et al. (2021), and Muroi et al. (2024) conducted differential lidar analyses along other sections of the 2016 rupture, there has been no study to estimate the amount of displacement in the area of slip partitioning between the Futagawa and Idenokuchi faults. Additionally, we conduct a paleoseismic trenching investigation of the Idenokuchi fault. We document the paleoseismic history of the Idenokuchi fault and compare our results with those of the Futagawa and Miyaji faults. Our findings indicate that all three faults could have ruptured together multiple times in the past, providing insight into understanding the interaction of multiple faults in complex ruptures. These results also have implications for assessing displacement hazards associated with slip partitioning on secondary faults.

2 Regional setting

Kyushu Island is part of the Southwest Japan arc and is the southernmost of the four main islands of the Japanese archipelago (Fig. 1). It is located on the Eurasian Plate, beneath which the Philippine Sea Plate

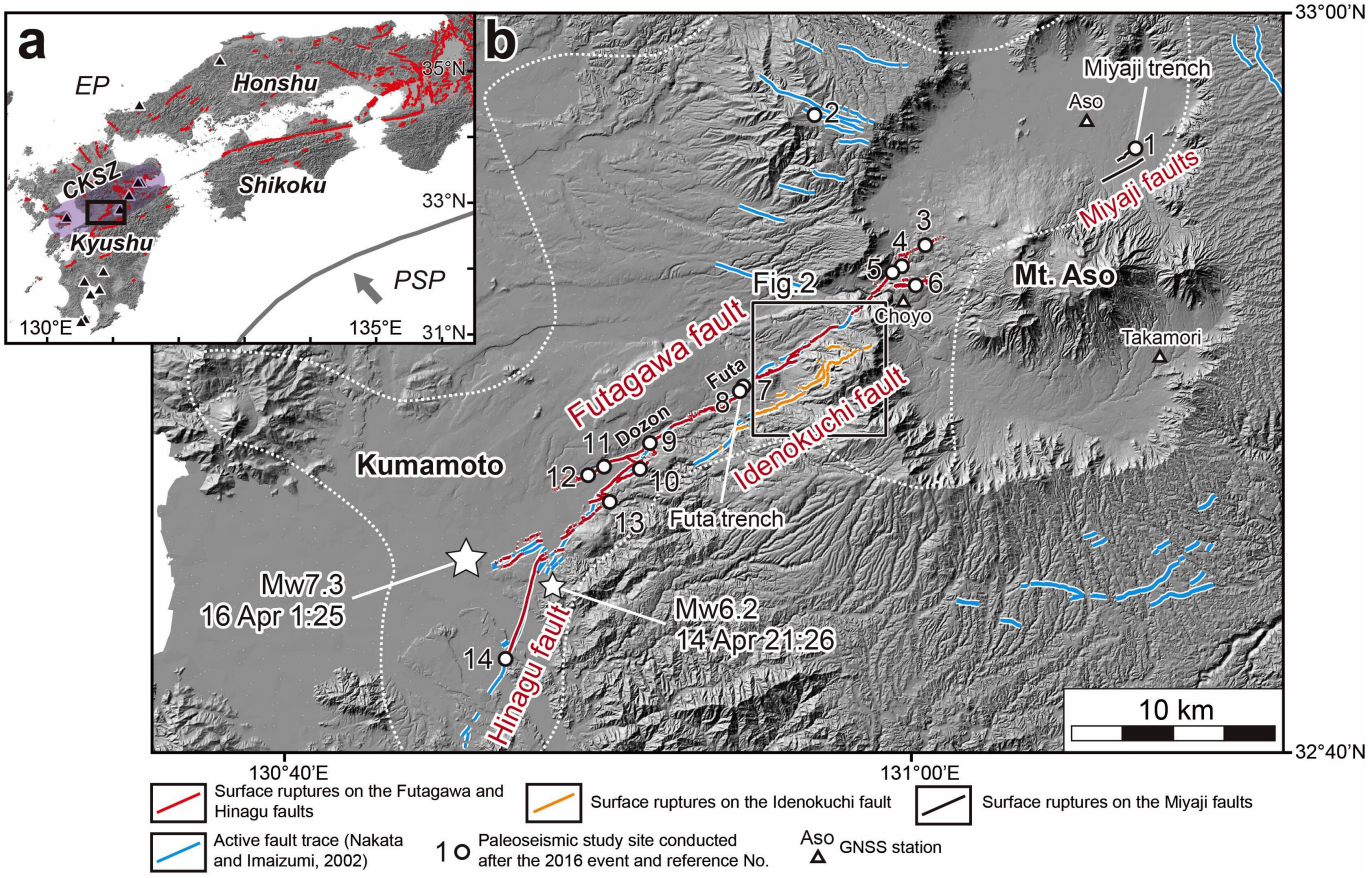

Figure 1 Spatial relationships among the primary Futagawa–Hinagu rupture zones and previously mapped active fault traces. (a) Tectonic setting, active volcanoes, and active faults in southwest Japan. CKSZ: Central Kyushu Shear Zone (Oohashi et al., 2020). EP: Eurasian Plate. PSP: Philippine Sea Plate. (b) Locations of the surface ruptures along the Futagawa, Hinagu, Idenokuchi, and Miyaji faults. The surface rupture traces are from Kumahara et al. (2022). Previously mapped active fault traces are from Nakata and Imaizumi (2002). Red and orange lines indicate primary and subsidiary surface ruptures, respectively, as defined in this study. The dotted line encloses the area where secondary surface ruptures were identified by InSAR (Fujiwara et al., 2016). The Miyaji faults (Ishimura et al., 2021) are examples of the many secondary surface ruptures associated with the 2016 event. In this study, we defined the Kiyama, Futagawa, and Kitamukiyama faults, previously mapped by the Research Group for Active Faults of Japan (1991), as the Futagawa fault. 1: Ishimura et al. (2021), 2: Sato et al. (2021), 3: Ueta et al. (2018), 4: Toda et al. (2019), 5: Kumahara et al. (2017b), 6: Okamura et al. (2018), 7: Iwasa et al. (2022), 8: Ishimura et al. (2022), 9: Kumahara et al. (2017b), 10: Takahashi et al. (2017), 11: Tsutsumi et al. (2018), 12: Ueta et al. (2018), 13: Inoue et al. (2020), 14: Shirahama et al. (2021).

is subducting northwestward at an oblique angle (Seno et al., 1993). Kyushu is characterized by many active volcanoes that have produced numerous tephra layers with well-established ages (Table S1; Machida and Arai, 2003; Miyabuchi, 2009). Active faults are primarily concentrated in the central and northern regions of Kyushu (Research Group for Active Faults of Japan, 1980, 1991).

The central Kyushu region has been deformed by north-south extension since 6 Ma (Kamata and Kodama, 1994), and is structurally characterized by the Beppu-Shimabara graben (Matsumoto, 1997). This area is characterized by many east-west-striking normal faults (Research Group for Active Faults of Japan, 1991) and high levels of volcanic activity. According to Oohashi et al. (2020), central Kyushu has been a transtensional tectonic zone since approximately 1 Ma, referred to as the Central Kyushu Shear Zone (Fig. 1), characterized by dextral faults, rift zones, and volcanism.

2.1 Futagawa fault zone

The Futagawa fault (Fig. 1) is a ca. 25-km-long active dextral strike-slip fault (Watanabe and Ono, 1969; Research Group for Active Faults of Japan, 1980, 1991; Nakata and Imaizumi, 2002; Kumahara et al., 2017a; Suzuki et al., 2017) and generated the mainshock (Mw 7.0) of the 2016 Kumamoto earthquake sequence on April 16, 2016. Primary surface ruptures appeared during the mainshock along the previously mapped active fault traces (Fig. 1; Kumahara et al., 2022). Dextral displacements of about 2 m were observed between Dozon and Futa along the central part of the Futagawa fault, with a maximum dextral displacement of 2.5 m at Dozon (Fig. 1; Shirahama et al., 2016; Okamura et al., 2018; Kumahara et al., 2022). Vertical displacement of about 1 m (south up) was observed along the central and western parts of the Futagawa fault (Shirahama et al., 2016; Okamura et al., 2018; Kumahara et al., 2022). The right-lateral and vertical slip rates for the Futagawa fault

determined near Futa are 1.5–3.7 mm/yr and 0.9–1.1 mm/yr, respectively (Ishimura et al., 2019).

The Idenokuchi fault is a 10-km-long active dip-slip fault primarily up on the south (Research Group for Active Faults of Japan, 1980, 1991; Nakata and Imaizumi, 2002), and also ruptured the surface during the mainshock of the 2016 Kumamoto earthquake (Fig. 1; Kumahara et al., 2022). Surface ruptures occurred along multiple subparallel faults. The maximum vertical displacement was 2 m (south up), and the average vertical displacement was about 1 m (Kaneda et al., 2022). Toda et al. (2016) inferred that the vertical slip on the Idenokuchi fault was related to the slip partitioning of the oblique lateral slip on the Futagawa fault. There is no data on the slip rate of the Idenokuchi fault.

2.2 Previous paleoseismic survey along the Futagawa fault

Extensive paleoseismic trenching has been conducted along the Futagawa fault and its vicinity since the 2016 event (Fig. 1). They are divided into three types: 1) on the surface ruptures along the primary Futagawa fault (Kumahara et al., 2017b; Takahashi et al., 2017; Okamura et al., 2018; Tsutsumi et al., 2018; Ueta et al., 2018; Toda et al., 2019; Ishimura et al., 2022; Iwasa et al., 2022), 2) on the surface ruptures along the Hinagu fault (Shirahama et al., 2021), and 3) on other secondary surface ruptures (Inoue et al., 2020; Ishimura et al., 2021; Sato et al., 2021). Almost all of these studies identified multiple events in the Holocene. Some studies estimated the age of the penultimate event on the primary Futagawa fault to be about 2 ka (Ueta et al., 2018; Toda et al., 2019; Iwasa et al., 2022; Ishimura et al., 2022). Comparison of paleoseismic information obtained after the earthquake with that before the earthquake (Headquarters for Earthquake Research Promotion, 2013) suggests that the Futagawa fault has been more active at least during the Holocene than previously assessed before 2016.

3 Methods and data

3.1 Lidar differencing

We used a 2-m grid DTM surveyed from January 2013 to February 2014 and a 2-m grid DTM surveyed on May 2016. Although we do not possess the original point cloud data of pre- and post-earthquake datasets, nor the details for constructing the DTMs from the original point cloud data, all the DTMs were prepared under the regulations required for a public lidar survey in Japan. We used the Japan plane rectangular coordinate system II (in meters) as the coordinate system for all data.

We applied the 3D-Geomorphic Image Velocimetry method (Kokusai Kogyo Co., Ltd., JP Patent No. 4545219, 2010) for lidar differencing. The particle image velocimetry method and pre- and post-event DTMs (Fig. 2) were used to calculate the surface displacement vectors following the methods of Mukoyama (2011) and Ishimura et al. (2019). Aoyagi et al. (2021) and Muroi et al. (2024) used this method for the eastern extension of the Futagawa fault inside the Aso caldera. The method procedure is as follows. First, we prepared slope-shaded images using pre- and post-event DTMs. We then carried out a grid search by moving a pre-event image in a pixel-by-pixel manner in the scanning area on the post-event image and estimated the position that exhibited the highest value of the coefficient of correlation using subpixel interpolation. From this step, we used the head and tail of each horizontal vector to calculate the two horizontal components (north-south and east-west) of displacement and estimate the vertical component using the elevation values at head and tail positions from DTMs. Subsequently, we slid the search area in steps and repeated the image matching and calculation of the 3D displacement. Finally, we plotted the complete 3D vectors on maps. In this study, the search area size, search area step size, and output grid size were set to be 64 x 64 pixels (128 x 128 m), 5 m, and 5 x 5 m, respectively. Additionally, the theoretical error of this analysis is 0.1 pixel (0.2 m) due to subpixel interpolation in the displacement calculation.

The expected ground motions during the measurement period are as follows: (1) the deformation associated with the 2016 Kumamoto earthquake, (2) the postseismic deformation (e.g., aftershocks and afterslip), (3) the background tectonic deformation, and (4) the artificial modification and present-day surface processes. We evaluate the deformation of items 2 and 3 using the GNSS observations in the study area. Based on the GNSS stations at the Choyo (960701), Aso (960703), and Takamori (960704) of GeoNET, the postseismic and background deformations (vertical, north-south, and east-west components) from April 2010 to May 2016 are nearly equal to the theoretical error level (0.2 m). Thus, the deformations associated with items 2 and 3 are negligible. Regarding item 4, although the impact varies from location to location, it is not possible to distinguish between phenomena caused by earthquakes and those not caused by earthquakes, based on the analyses of aerial photographs and the topography. Therefore, in this study, we avoid using data from such locations for interpretation (e.g., surface failures and areas with artificial modifications).

3.2 Trench survey

We looked for an appropriate site for a paleoseismic excavation along the Idenokuchi fault (Figs. 2 and 3). We selected possible sites based on the following criteria: 1) minor artificial modification, 2) clear surface rupture traces, and 3) stable and continuous sediment deposition. As a result, we selected a trench site on a gentle slope characterized by subparallel fault traces of the Idenokuchi fault, expecting trapped sediment and stable and continuous soil deposition (Fig. 3). The trench site is on an apparent single surface rupture (north-up normal fault), and another surface rupture (south-up normal fault) runs parallel on its southeast side. Currently, the fields are cow ranches with minor artificial modification.

We excavated a 13-m-long, 5-m-wide, and 3.5-m-deep trench (Fig. 3; KMR trench) and established a grid system on the trench walls. We logged the walls and col-

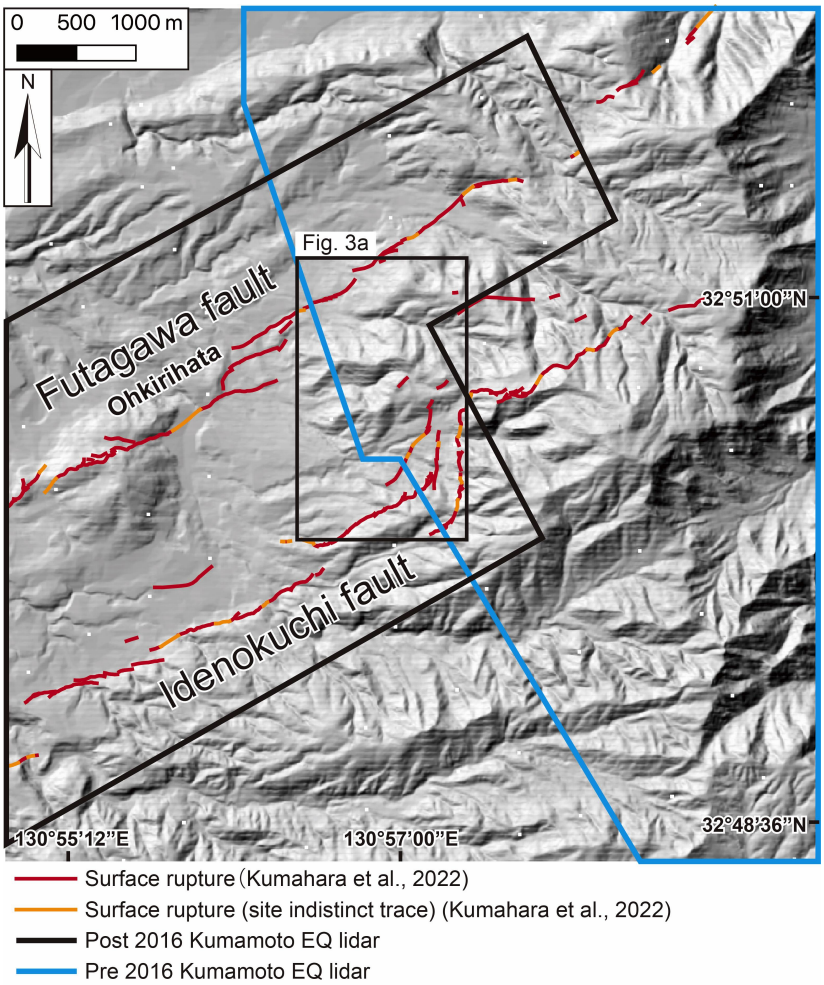

Figure 2 Extent of lidar data used to measure displacements and surface ruptures. Lidar survey areas include the post-2016 Kumamoto earthquake (black polygon) and pre-2016 Kumamoto earthquake (blue polygon).

lected samples for tephra analyses and radiocarbon dating. To further examine the subsurface geology, we used a 50-cm-long and 4-cm-wide corer to obtain seven cores from the trench floor and the upthrown side (Fig. S1). We used a Nikon Nivo5.SC total station to map the locations of the surface ruptures, trench, and coring sites (Fig. 3b).

3.3 Laboratory analysis

We determined refractive indices and major element compositions of volcanic glass shards in the sampled tephras. First, we sieved the samples with water through a 62-µm nylon mesh. Then, we oven-dried the samples at 50˚C and sieved the dried samples through a 120-µm nylon mesh. The refractive index of volcanic glass shards in the 62–120 µm fraction of each sample was measured with a RIMS 2000 refractive index measuring system (Kyoto Fission Track Co., Ltd.) with an accuracy of ±0.0002 (Danhara et al., 1992). The major element composition of volcanic glass shards was measured by an energy-dispersive X-ray spectrometry (EDAX Genesis APEX2 and JEOL JSM-6390) following the method and analysis conditions described by Suzuki et al. (2014). Volcanic glass shards of the AT tephra sampled at Chigaki, Toyama Prefecture (Machida and Arai, 2003) were used as a working standard to check data reproducibility and instrument stability. A total of 12 tephra samples from the trench walls were analyzed and compared to two reference samples (Tables S2, S3, and S4).

A total of 26 radiocarbon samples, including charcoal and organic sediment (Table S5), were dated by accelerator mass spectrometry at the Laboratory of Radiocarbon Dating, University Museum, University of Tokyo, and the Institute of Accelerator Analysis Ltd., Japan. The obtained ages were calibrated using the OxCal 4.4 software (Ramsey, 2008) with the IntCal20 dataset (Reimer et al., 2020). The ages of paleofaulting events were calculated in the OxCal program by Bayesian analysis (Ramsey, 2008).

4 Results

4.1 3D displacement analysis

Figure 4 shows the distribution of 3D displacements during the 2016 earthquake, and Figure 5 shows topographic displacement profile lines A-D. In the profile lines (Fig. 5), the horizontal component is divided into two parts: parallel to the general strike of the Futagawa fault (N57°E) and perpendicular to it. The vertical component (Figs. 4c and 5) shows a displacement of 1.0–2.5 m at the southernmost part of the Idenokuchi fault and

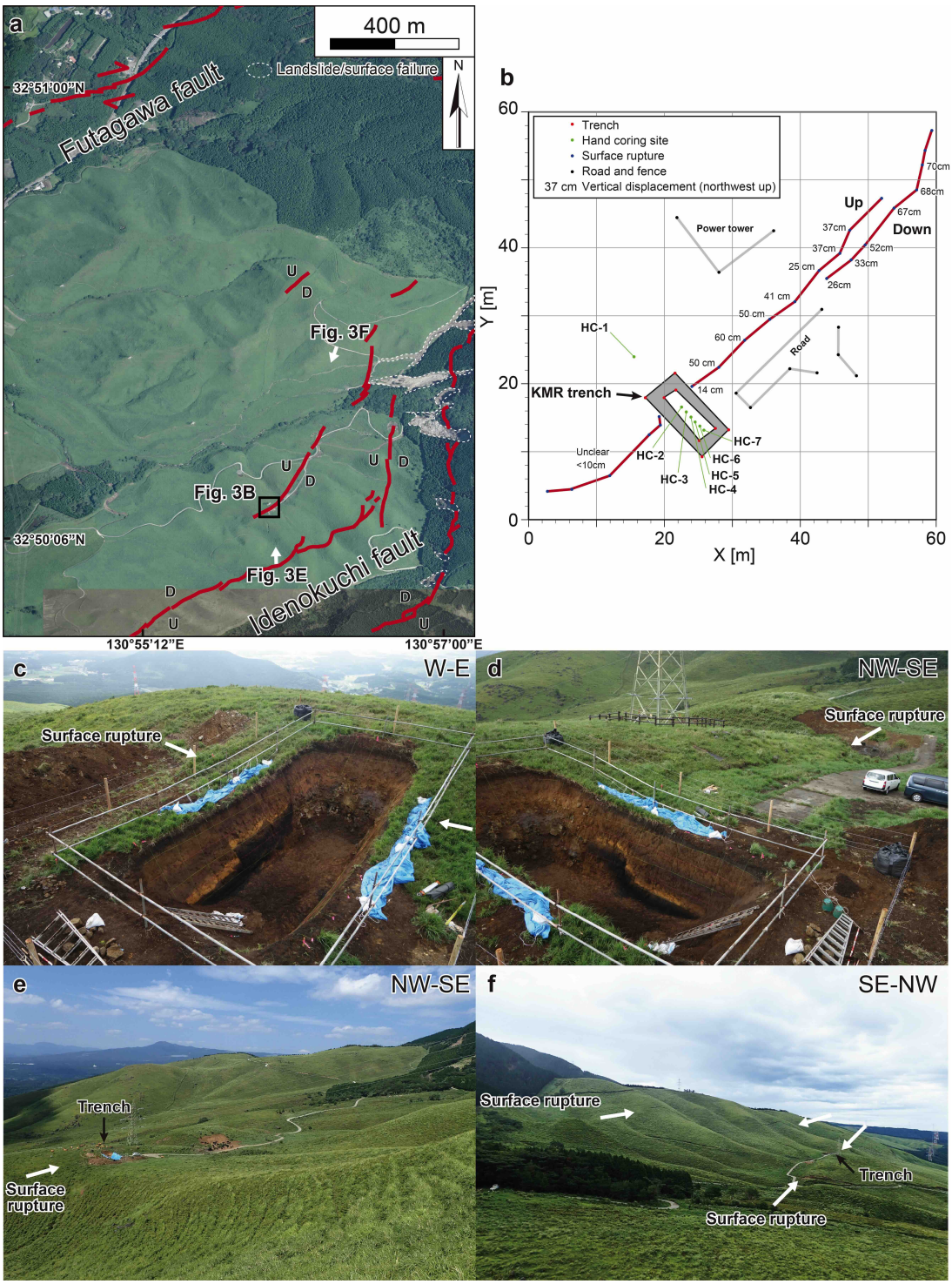

Figure 3 Geomorphic map and photographs around the trench site. (a) Red lines show the 2016 surface ruptures (Kumahara et al., 2022). Aerial photograph from the Geospatial Information Authority of Japan. (b) Location map of the trench and surface ruptures. Numbers indicate vertical displacement measurements. (c) Photo of the west wall of the trench. (d) Photo of the east wall of the trench. (e,f) Photos of geomorphic conditions around the Idenokuchi fault trench site. Photo locations are shown in Fig. 3a.

a vertical displacement of several tens of centimeters at the northern part of the fault. Compared to field measurements (Kaneda et al., 2022), a similar displacement was observed along the southernmost branch of the Idenokuchi fault, where a 2 m vertical displacement was recorded. However, the amount of vertical displacement along the fault is noisy and subject to uncertainty because of slope failures in the surrounding area. Along the parallel splay of the Idenokuchi fault, where we excavated the KMR trench, there is no significant difference between the calculated and field-measured displacements. On the other hand, on the Futagawa fault, the amount of local vertical displacement associated with the dextral displacement is observed in a narrow section about 200 m wide. When viewed over a 200–400 m wide zone from the fault, little difference

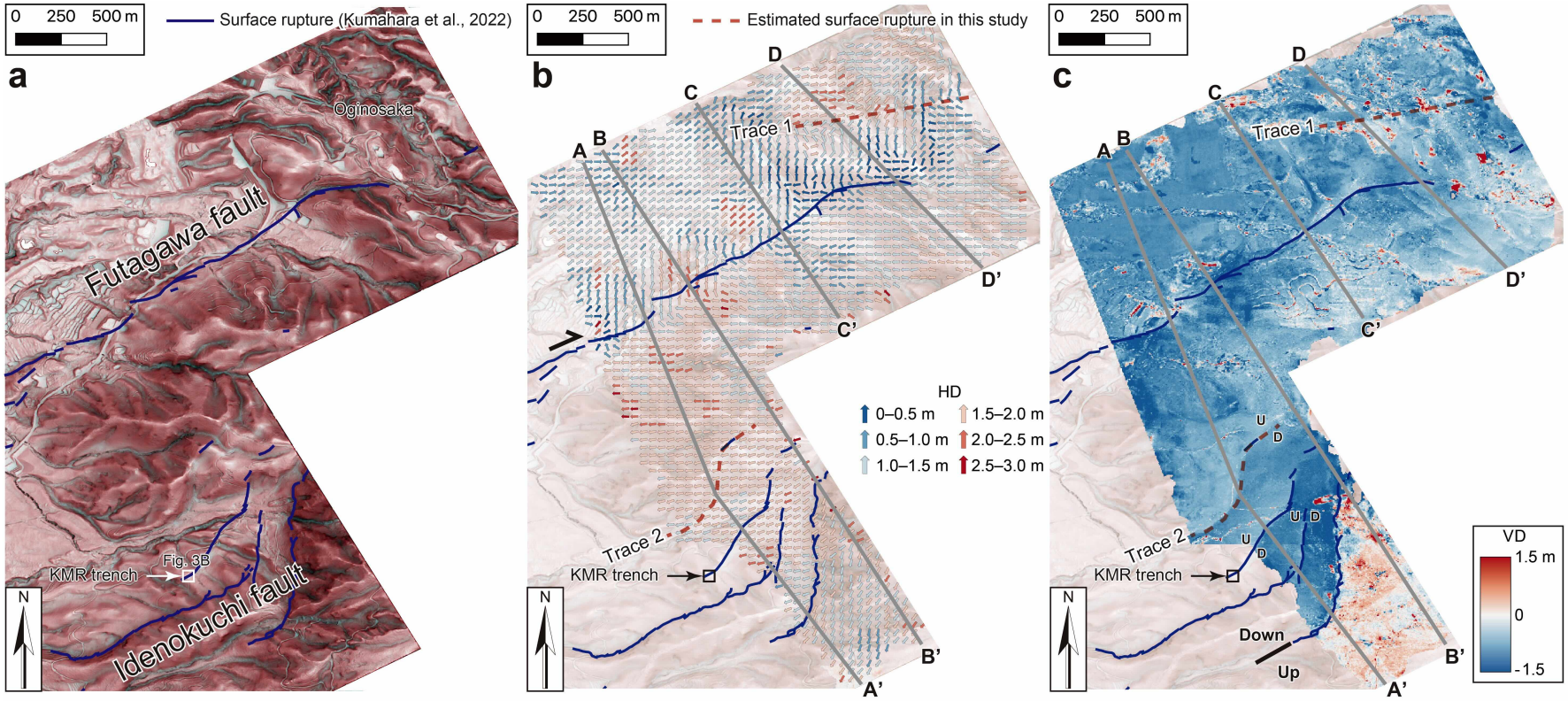

Figure 4 Results of the differential lidar analysis. (a) Red relief image map around the study area. The map was created following the methods of Kaneda and Chiba (2019). Surface ruptures are after Kumahara et al. (2022). (b) Horizontal displacement field. Horizontal displacement is indicated by the arrow and color. (c) Vertical displacement field. Vertical displacement is shown by the color map. HD: horizontal displacement, VD: vertical displacement. Letters (i.e., A-A') indicate endpoints of displacement profiles shown in Fig. 5.

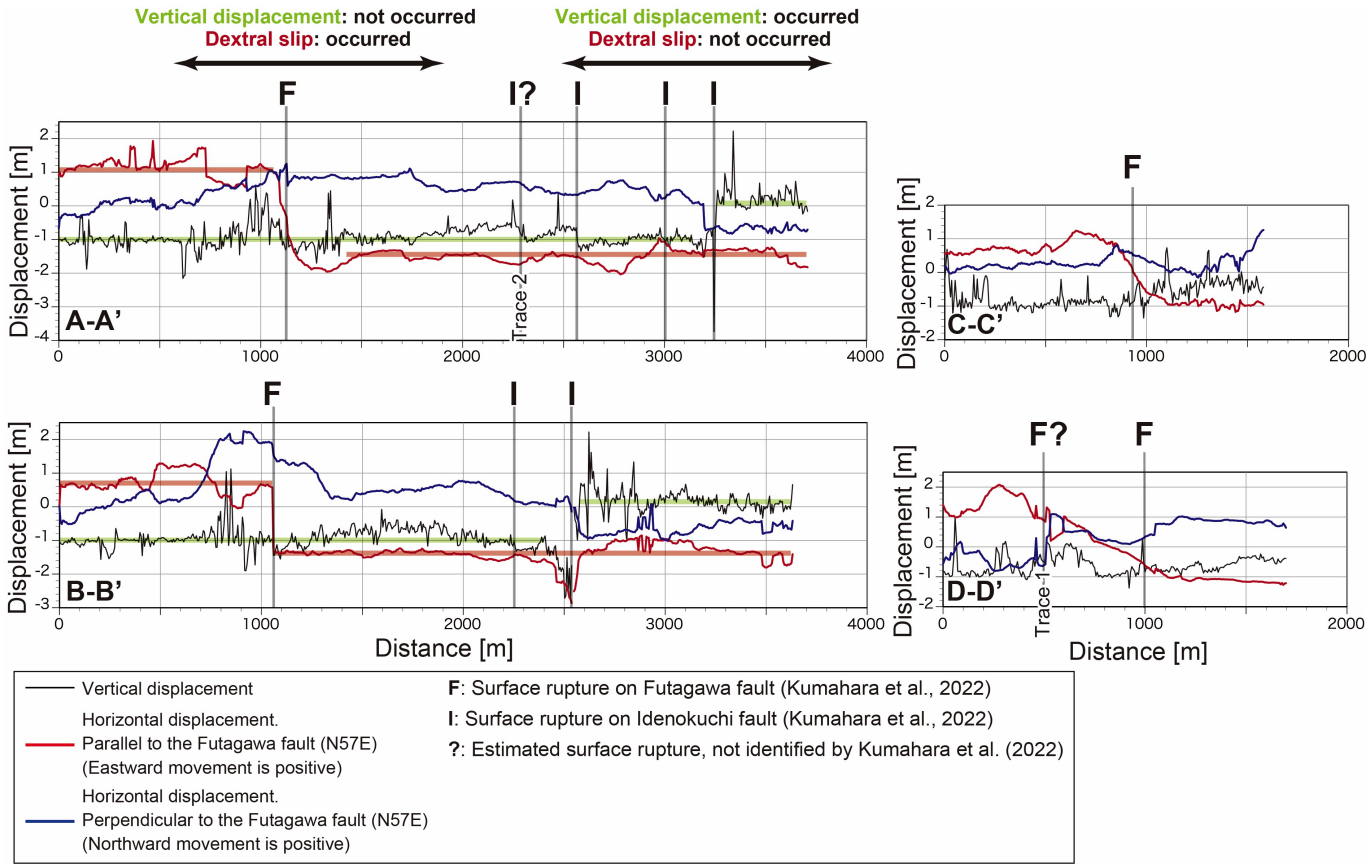

Figure 5 Vertical and horizontal displacement profiles. The profile lines are shown in Fig.4.

in vertical displacement across the Futagawa fault is observed. The vertical displacement along the long baseline (>3 km) extending across both the Futagawa and Idenokuchi faults is about 1 m south-up (Lines A and B in Fig. 5).

A large fault-parallel displacement was observed on the Futagawa fault, and 1.8–3.1 m of dextral displacement occurred on the western part of the calculated area (Figs. 4b and 5). Since the displacement measured in the field was approximately 1.5–2.0 m (Shirahama et al., 2016; Kumahara et al., 2022), the 3D displacement data can be used to determine both the amount of off-fault and on-fault displacements. This trend has also been discussed by Scott et al. (2018). In the western part of the Futagawa fault, larger dextral displacements were obtained for the long baseline (1 km) compared to the short baselines (35 m and 100 m). Although it is difficult to identify from the 3D displacement distribution map (Fig. 4b), a slight sinistral displacement occurred on the Idenokuchi fault, which is consistent with the field measurements (Toda et al., 2016; Shirahama et al., 2016; Kaneda et al., 2022). In the eastern half of the calculation area, the contrast in displacement is smaller, the amount of displacement decreases, and there is greater variability because surface failures and other factors may have also occurred. The dextral displacement along the long baseline (>3 km) between both faults is about 2–2.5 m.

Regarding the fault-perpendicular component (Fig. 4b and A-A' and B-B' in Fig. 5), extension occurred locally on the Idenokuchi fault, and shortening occurred locally on the Futagawa fault. The extension is large at the southernmost part of the Idenokuchi fault, with a displacement of about 1–1.5 m. A shortening of about <1 m occurred on the Futagawa fault. The displacement in the perpendicular direction of the fault along the long baseline (> 3 km) across both faults is approximately 1 m of extension.

The 3D displacement observations and field measurements are generally in agreement in terms of the locations of surface ruptures and the amount and sense of displacements. However, in two locations, surface ruptures were inferred from the displacement data but have not been confirmed in the field (Trace 1 and Trace 2; Figs. 4b and 4c). Trace 1 occurs north of the Futagawa fault in the eastern part of the calculated area. Here, slight contrasts in fault parallel and perpendicular components are observed. Although it is unclear whether these displacements are associated with a well-defined fault, the discontinuity projects towards a surface rupture that continues eastward into the caldera (Kumahara et al., 2022). It also coincides with a 2 m shortening identified at a bridge abutment near Oginosaka (Fig. 4; Shirahama et al., 2016). Trace 2 is a north-up displacement recognized along the northernmost splay of the Idenokuchi fault. Here, a short surface rupture was recognized (Kaneda et al., 2022), and it is likely to extend further to the southwest. Regarding the vertical component, a clear difference is observed on both the plan view and the profile on either side of Trace 2 (Figs. 4c and 5). On the other hand, the horizontal components are somewhat less distinct. Trace 2 coincides

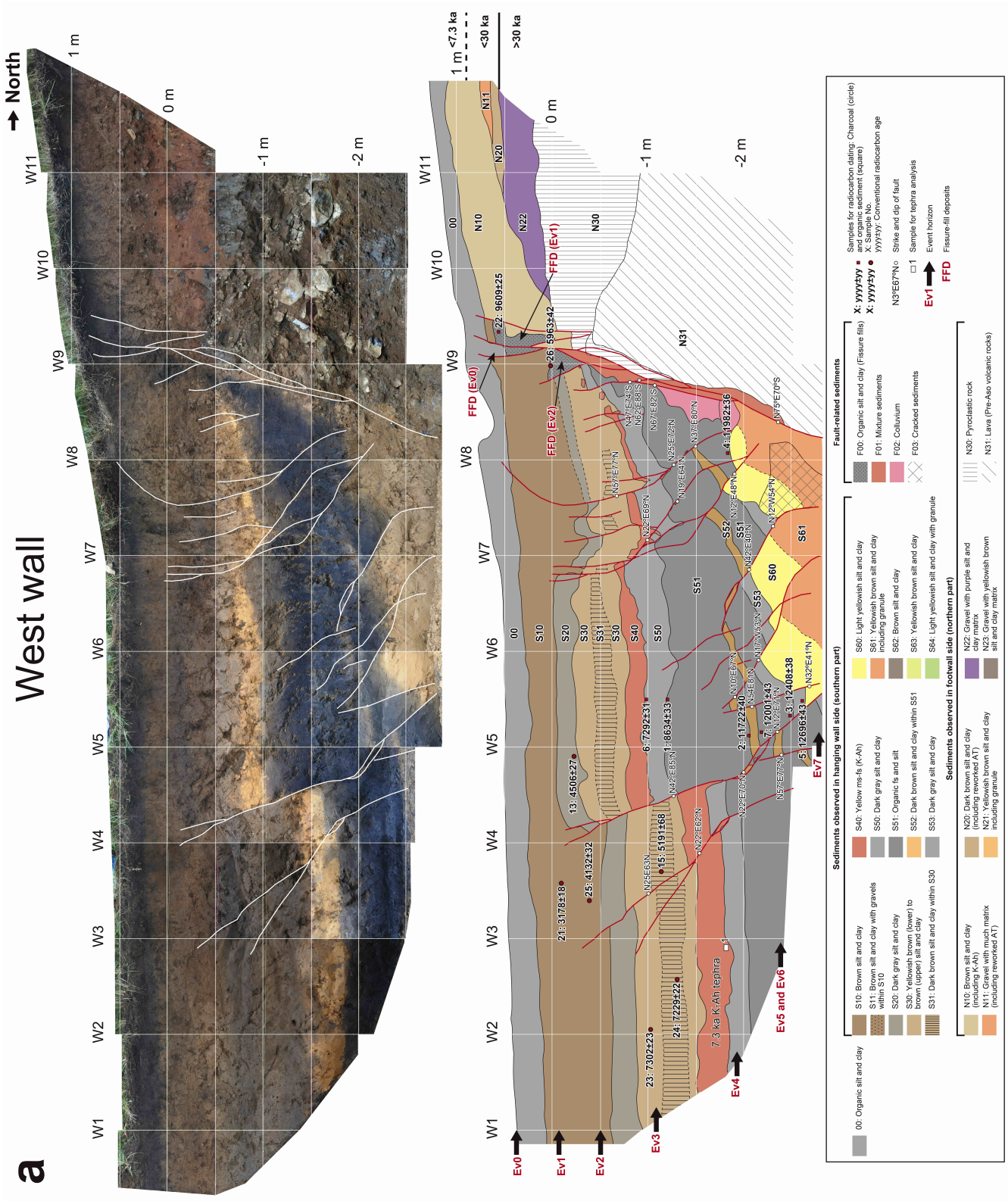
a
West wall
North
W1
W2
W3
W4
W5
W6
W7
W8
W9
W10
W11
1 m
0 m
-1 m
-2 m
<7.3 ka
<30 ka
>30 ka
FFD (Ev0)
FFD (Ev1)
FFD (Ev2)
Ev0
Ev1
Ev2
Ev3
Ev4
Ev5 and Ev6
Ev7
7.3 ka K-Ah tephra
Sediments observed in hanging wall side (southern part)
Sediments observed in footwall side (northern part)
Fault-related sediments
Samples for radiocarbon dating: Charcoal (circle) and organic sediment (square)
X: Sample No.
yyyy±yy: Conventional radiocarbon age
Strike and dip of fault
Sample for tephra analysis
Event horizon
Fissure-fill deposits

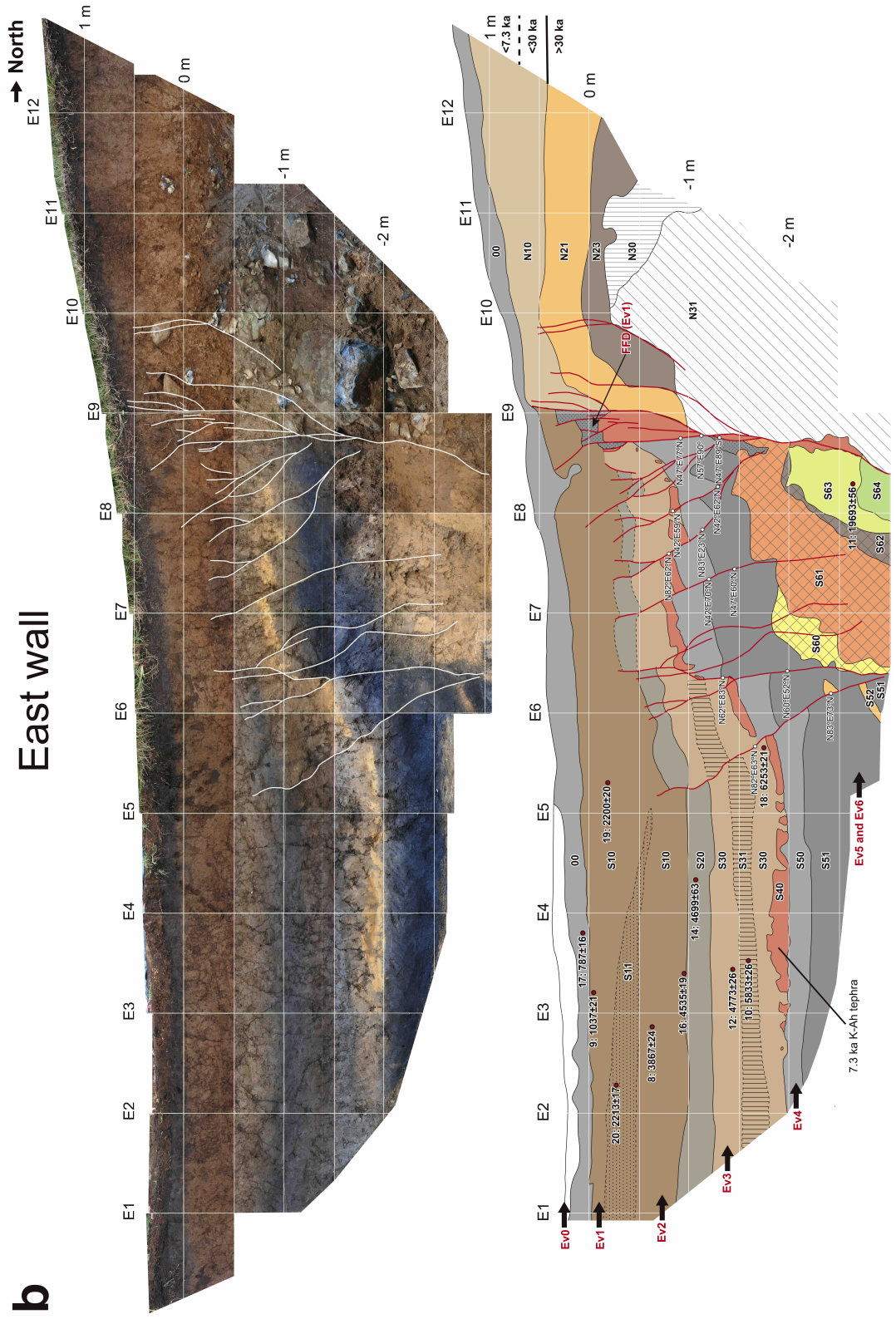
b
East wall
North
E1
E2
E3
E4
E5
E6
E7
E8
E9
E10
E11
E12
1 m
0 m
-1 m
-2 m
<7.3 ka
<30 ka
>30 ka
FFD (Ev1)
Ev0
Ev1
Ev2
Ev3
Ev4
Ev5 and Ev6
7.3 ka K-Ah tephra
00
N10
N21
N23
N30
N31
S10
S11
S20
S30
S31
S40
S50
S51
S52
S60
S61
S62
S63
S64
9: 1037±21
16: 4535±19
14: 4699±63
12: 4773±26
10: 5833±26
18: 6253±21
19: 2200±20
17: 787±16
8: 3867±24
20: 2213±17
11: 19693±56

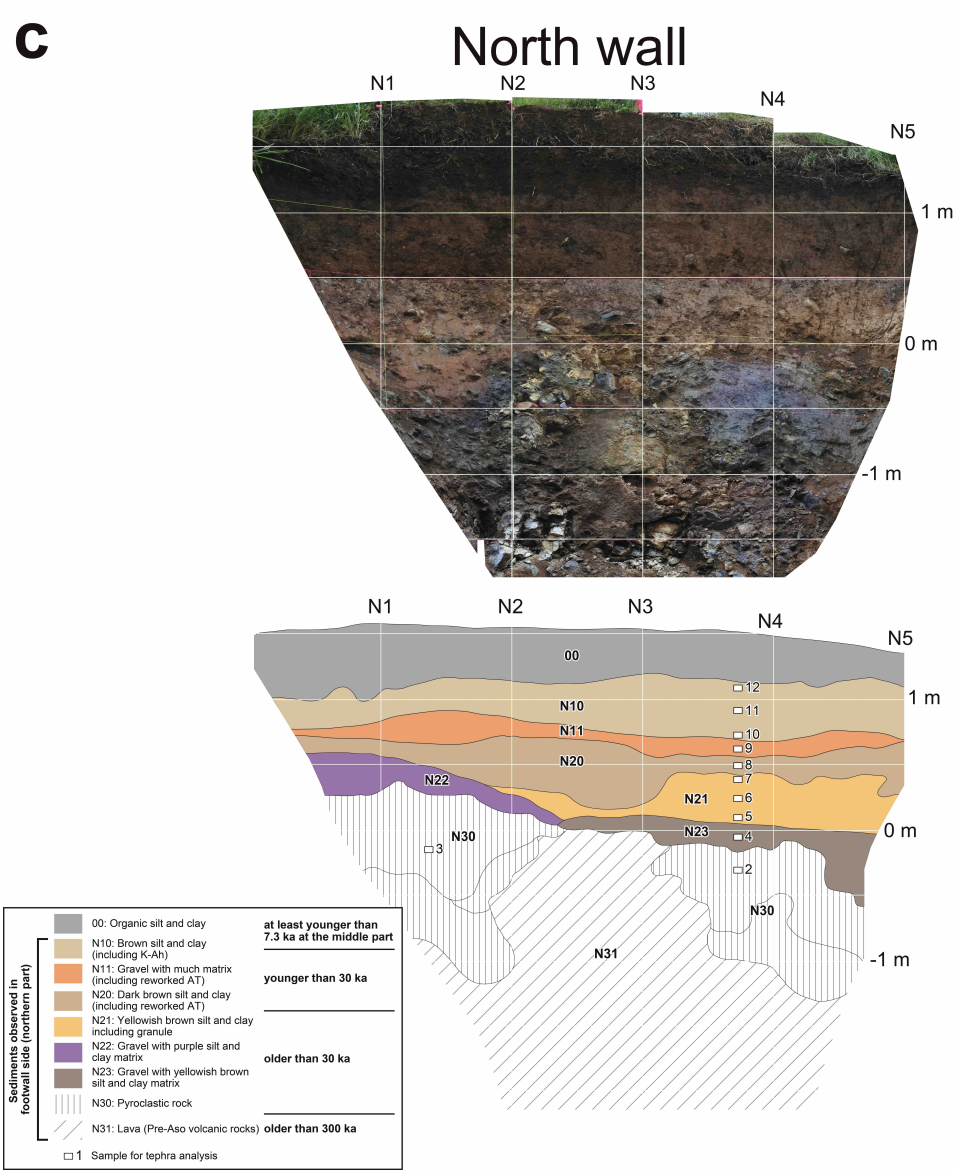

Figure 6 Photomosaics and sketches of the stratigraphic and structural relations exposed in the KMR trench walls. (a) West wall. (b) East wall. The sketch of the east wall is flipped. Legend shown in (a) applies to both the west and east walls. (c) North wall. FFD: fissure-fill deposits.

with the present valley topography and may have been affected by fluvial erosion and other factors during the DTM measurement period.

4.2 Paleoseismic trench

4.2.1 Trench stratigraphy (including tephra analysis)

The trench exposed a package of silts, clays, and paleosols, separated from gravels and bedrock, across the primary normal fault. Figure 6 shows photomosaics and sketches of the west, east, and north walls. In this trench, sediments with different sedimentary facies and ages accumulated on the north (footwall, upthrown side) and south (hanging wall, downthrown side) sides across the primary normal fault at W9/E9. For this reason, the footwall and hanging wall sediments are assigned different unit numbers except for the topsoil (unit 00), which extends across the entire exposure.

Sediments exposed in the south side of the trench (hanging wall) were deposited relatively continuously (Figs. 6a and 6b) and are described from youngest to oldest. Unit 00 is the topsoil, consisting of black, organic silt and clay. Unit S10 is a thick, brown silt and clay below unit 00. On the east wall, an interbed within unit S10 consisting of gravelly clay was classified as unit S11. Unit S20 is a dark gray silt and clay and is considered an organic-rich paleosol. Unit S30 is a yellowish brown to brown silt and clay with a slightly darker interbed (unit S31), which is an organic-rich paleosol similar to unit S20. Both Units S30 and S31 slightly thicken to the south away from the primary normal fault. Unit S40 is composed of fine to medium yellow sand, mainly composed of volcanic glass that is bioturbated and discontinuous in places. Units S50 and S51 are organic-rich paleosols. Unit S50 is dark gray silt and clay, and unit S51 is organic silt and fine sand, with unit S50 slightly lighter in color than unit S51. Unit S52 is yellowish brown to brown silt and clay interbedded within unit S51. Unit S53, which is observed only on the west wall, is a slightly lighter gray

silt and clay similar to unit S50. Unit S53 has an undulating basal contact suggesting an unconformity with unit S60 on the west wall. Unit S60 is a bright yellowish silt and clay, and unit S61 is a yellowish-brown silt and clay with granules. On the west wall, unit S61 is the lowest (oldest) deposit. On the east wall, unit S61 is underlain by brown to yellowish brown silt and clay (units S62 and S63). The basal deposit (unit S64) is a light yellowish silt and clay with granules.

Sediments exposed in the north side of the trench (footwall) are thinner than those on the hanging wall and are primarily composed of gravel and rock (Fig. 6). The footwall sediments are slightly different between the east and west walls, and are thus described from the north trench wall which exposed the entire footwall package (Fig. 6c). Unit N10, consisting of brown silt and clay, has an erosional relationship with the underlying unit N11 and lower units (see west wall in Fig. 6a). Unit N11 is a matrix-supported gravel bed. Units N20 and N21 are dark brown and yellowish-brown silt and clay, respectively. Both units N22 and N23 are matrix-supported gravel beds that vary in color from purple to yellowish brown. Unit N30 is a pyroclastic rock unit with an undulating and irregular basal contact. Unit N31 is composed of fragmented lava from pre-Aso volcanic rock, which forms the basement rock of the surrounding area (Hoshizumi et al., 2004).

To further explore the site stratigraphy, a transect of cores was advanced into the floor of the trench on the hanging wall (cores HC-2 to HC-7) and beyond the limits of the trench on the footwall (core HC-1) (Fig. S1). Core HC-1 revealed nearly identical stratigraphy and thicknesses as that exposed on the trench walls, from which we infer that the sediments exposed on the north wall are distributed widely and uniformly on the northern side of the fault. On the downthrown side (HC-2 to HC-7), the black silt and clay and yellowish brown to brown silt and clay, corresponding to unit S51 and lower, were observed. No black soil, corresponding to units S51 to S53, was observed at depths greater than 1 m from the trench floor. Gravel and sand beds, not recognized on trench walls, were observed in some cores. However, no tephra layers were identified. On the other hand, sediments were in contact with high angles, and voids were observed in some cores, which we inferred to be faults. The primary normal fault was considered the boundary with the basement rock, so we inferred the normal fault at a depth where drilling was no longer possible.

4.2.2 Faults

In this trench, we identified faults, rootless faults, and cracks. Faults refer to discontinuities with apparent displacement that extend downward to the bottom of the trench. Rootless faults are those with apparent displacement but do not extend downward to the trench bottom. Cracks are those without displacement. Although we observed many cracks on the trench walls, we did not show them in the figures because they were interpreted to be related to drying of the walls and did not affect the paleoseismic interpretations. The primary normal fault is observed at W9/E9, and many other faults are rootless with bending in the lower part. Faults extending down to the trench bottom are the north-up normal faults at W9/E9 and the reverse faults at W3-W5 and E5-E6. Normal faults that form grabens develop at W7-W9 and E7-E10. The 2016 displacement was an open crack near W9/E9, which was already filled with sediments at the time of trench excavation. Similar open cracks and fissure fill deposits have been identified in the Futa trench at Futa (Fig. 1; Ishimura et al., 2022). However, no other distinct 2016 displacement (e.g., apparent vertical displacement) was observed on the trench walls. This is likely because the trench is located in an area of decreasing vertical displacement from northeast to southwest, where the 2016 displacement is small (<14 cm) and indistinct (Fig. 3b). Other fissure-fill deposits that may have formed prior to the 2016 event were also identified below the 2016 fissure-fill deposits. Measurements of the strike and dip of the faults on the trench walls indicate that the predominant strike is northeast to southwest, but some are north to south or east-northeast to west-southwest (Fig. 6). The northeast-southwest strike is consistent with the surface ruptures (Fig. 3b). The other strike directions suggest that subsidiary surface ruptures to the primary normal fault may have occurred in the past events.

4.2.3 Tephra analysis

We completed tephra analysis for unit S40 (sample No. 1) on the hanging wall as well as a suite of 11 samples (Sample No. 2 to No. 12) from the footwall (Table S2 and Fig. 6). The results of the tephra analysis are shown in Table S2, and the major element composition of volcanic glass shards is shown in Tables S3 and S4. The results show that unit S40 is composed almost entirely of bubble-wall-type volcanic glass shards, with a refractive index of 1.510-1.512 (mode: 1.511), suggesting that it correlates with the widespread tephra, Kikai-Akahoya (K-Ah; 1.505-1.513 (mode: 1.510-1.512) in Table S1), by the eruption of southern Kyushu at 7.3 ka (Machida and Arai, 2003; Smith et al., 2013). The chemical compositions confirmed this correlation (Table S3), consistent with the existing studies in the vicinity (e.g., Ishimura et al., 2022).

Volcanic ash analysis of the samples from the north wall (Samples No. 2 to No. 12) revealed no tephra layers. Therefore, we examined the volcanic glass content and refractive indices to determine if the samples contained volcanic glass shards of Aira-Tn (AT) (30 ka; Smith et al., 2013) and K-Ah tephras, which are commonly identified widespread tephras in this area (Table S1; Machida and Arai, 2003). The results (Table S2) show that there is almost no volcanic glass below unit N21, while units N20 and N11 exhibit very low volcanic glass content (2%). The refractive indices of volcanic glass are mainly 1.495-1.500 (mode: 1.497–1.499) (Table S2), which correlates with AT tephra (1.498-1.500 in Table S1). In contrast, the volcanic glass content increases from the lower to the upper part of unit N10. The refractive indices show that while unit N10 contains glass with a refractive index of 1.497-1.500 of AT origin, the percentage of volcanic glass of 1.508-1.512 of K-Ah origin increases toward the

upper part of unit N10. This suggests that the age of the middle part of unit N10 postdates the K-Ah tephra. This mixing of AT and K-Ah volcanic glass is also observed in soils in other regions, and the K-Ah ash fall horizon is roughly estimated at the peak of K-Ah volcanic glass shard content (Ishimura and Kakiuchi, 2011). Such distribution of volcanic glass shard content may be due to bioturbation and secondary deposition of tephra-origin particles. Based on the presence of AT volcanic glass, unit N20 is at least younger than 30 ka, and unit N21 and below are older than 30 ka. Based on the K-Ah glass content, the upper to middle part of unit N10 is interpreted to be at least younger than 7.3 ka. The fact that K-Ah tephra is exposed in the hanging wall indicates that sediment preservation potential is better on the downthrown side of the fault.

4.2.4 Radiocarbon dating

Because the faulting events described below were identified on the downthrown side of the primary normal fault, we performed radiocarbon dating of samples collected from the south side of both trench walls (Table S5). A total of 26 samples were analyzed. Sample locations and ages are shown on the trench logs (Fig. 6) and radiocarbon data are summarized in Table S5. The youngest age was 787 ± 16 yr BP (charcoal; Sample 17) from unit 00, and the oldest was 19693 ± 56 yr BP (charcoal; Sample 11) from unit S63. In general, the radiocarbon results are stratigraphically consistent (progressively older ages with depth, with only several exceptions explained below). For sediments older than unit S50, bulk samples (organic sediments) were dated except for the sample from unit S63. As Ishimura et al. (2022) pointed out, the ages of bulk samples in this region are sometimes younger than the actual ages. In this trench, we compared the bulk sample ages with the ages of the K-Ah tephra and the charcoal from unit S63. As a result, the bulk sample ages were consistent with the tephra and charcoal age, with no contradiction between the stratigraphy and age. Because we used charcoal samples above unit S30, it is possible that older charcoals were included by reworking, resulting in older ages. In such cases, charcoals with younger ages in the same unit were employed for further analyses. As a result, we did not use the ages, 7302 ± 23 yr BP and 7229 ± 22 yr BP from samples 23 and 24, respectively (Table S5). Additionally, the ages of bulk samples collected from the fissure-fill deposits (samples 22 and 26) were significantly older than the surrounding sediments. The specific organic matter responsible for the cause is unknown because they are bulk samples. One possibility is that the trench site is located on an uphill-facing scarp, acting as a trap for sediments, allowing old organic matter to deposit along faults and open fractures. In any case, it is thought that the fissure-fill deposits contained old organic matter. Therefore, the ages of these fissure-fill deposits are also not used.

4.3 Evidence for paleofaulting

We identified geologic evidence for faulting events since the deposition of unit S53 by stratigraphic evidence (Fig. 6) and retrodeformation (Figs. 7 and S2). Ev0 is the 2016 event, and an open crack occurred directly above the primary normal fault near W9/E9 (Figs. 6a and 6b). In Ev0, a further open crack was formed in the pre-existing open crack created by Ev1 (the penultimate event), which is described in the following paragraph. This Ev0 open crack was already filled with sediment at the time of our survey. Similarly, an open crack directly above the primary normal fault, located near E9, is recognized on the east wall (Fig. 6b). The surface rupture runs between W8-W9 and E8-E9, corresponding to the locations of open cracks. These observations confirm that the 2016 event formed these open cracks.

Ev1, like Ev0, developed an open crack directly above the primary normal fault near W9, which was immediately next to the open crack of Ev0 and filled by fissure-fill deposits. On the west wall, this fissure-fill deposit was formed in unit S10 during Ev1 and was displaced at the southern part by Ev0. Unit S10, displaced by Ev1, is stratigraphically positioned above unit S11, which may have been deposited by a slope failure in Ev2 as described in the following paragraph. Therefore, Ev1 is interpreted to have occurred during the deposition of unit S10, particularly after unit S11 deposition.

In Ev2, an open crack, normal fault displacements near the primary normal fault (W7-W9), and reverse fault displacements on the southern faults (W3-W4) occurred. Subsidiary normal and reverse faults displaced unit S20 and the lower part of unit S10, and a fissure-fill deposit was identified on the west wall (W9, 0 m). Therefore, this event occurred after the deposition of unit S20 paleosol and during the deposition of unit S10. Similarly, on the east wall, unit S20 was deformed by normal fault displacements near the primary normal fault (E7-E9), and reverse fault displacements across faults to the south (E5-E6). In addition, the gravel-rich unit S11 is recognized in unit S10 on the east wall, which is wedge-shaped and may be a deposit supplied from the southern slope, rather than from the main normal fault in the trench. A similar surface failure occurred in the southern slope along the Idenokuchi fault during the 2016 earthquake (Fig. 3a). Unit S11 is stratigraphically above the basal part of unit S10 and the faulted S20 deposit. Therefore, unit S11 may be a post-earthquake deposit related to Ev2. Thus, the event horizon of Ev2 is inferred to be after unit S20 and before unit S11.

Ev3, like Ev2, involved normal fault displacements near the primary normal fault (W7-W9) and reverse fault displacements on the southern faults (W3-W4). The east wall similarly shows normal fault displacements at E7-E9 and reverse fault displacements of the southern faults (E5-E6). On the east wall, even after restoring the fault displacement of Ev2, vertical displacement was still observed in faults at E6-E8 (Fig. S2). This indicates cumulative displacement, suggesting fault activity between units S20 and S40. The fault at W3 displaces unit S31, but does not displace unit S20. Therefore, the event horizon of Ev3 is inferred to be between units S20 and S31.

Ev4 is indistinct on the west wall, while it is distinct on the east wall. On the east wall, even after restoring the fault displacement of Ev2 and Ev3, vertical displace-

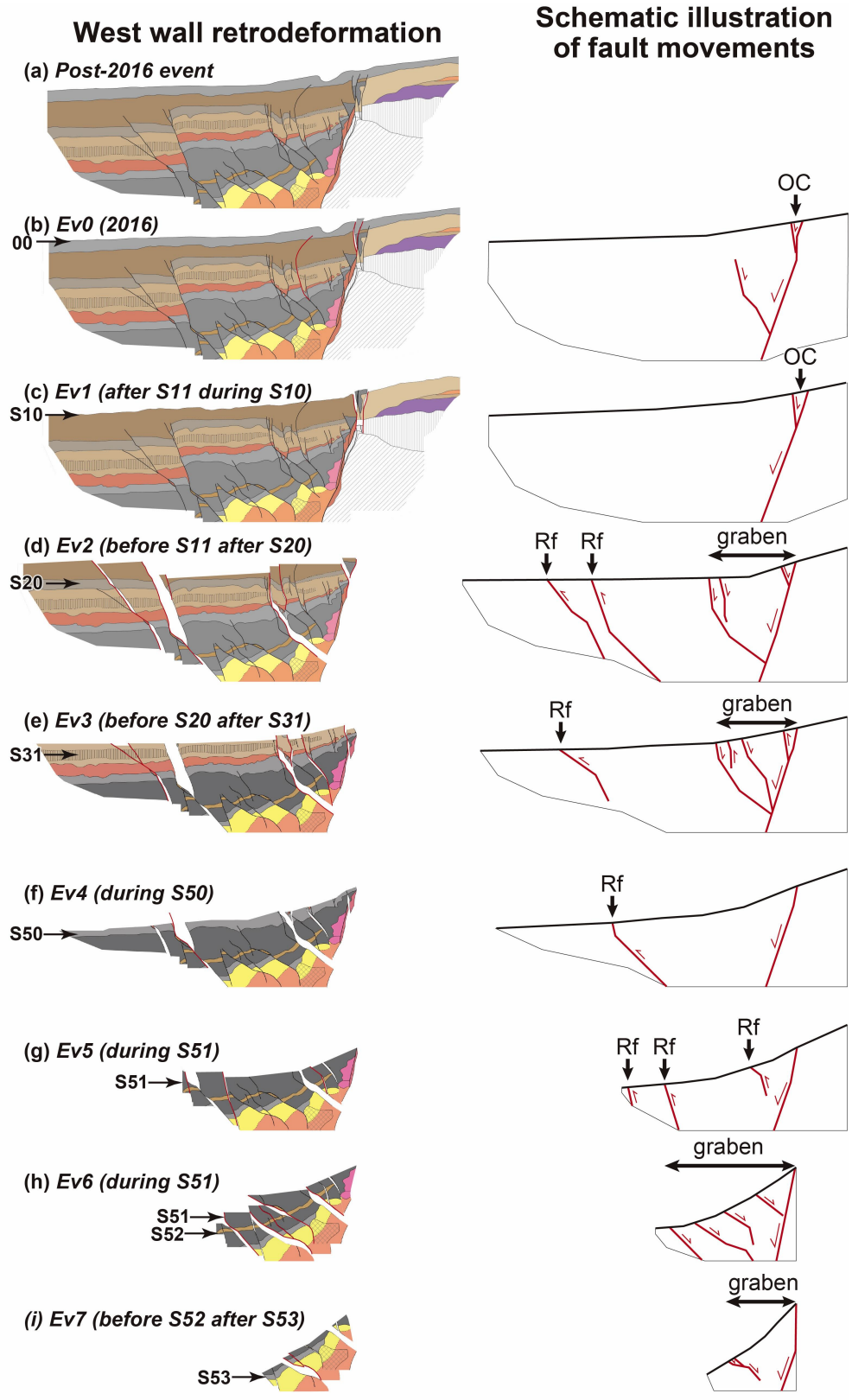

Figure 7 Retrodeformation of the faults and deformed strata, and schematic illustration of fault movements on the west wall. The left figures show reconstructions of the displacement for each event, and the right figures show the faults that were active during each event. Rf: reverse fault, OC: open crack.

ment was still observed for the reverse fault at E6 and normal fault at E8-E9 (Fig. S2). This indicates cumulative displacement, suggesting fault activity between units S40 and S51. Therefore, the event horizon of Ev4 is inferred to be during the deposition of unit S50.

Ev5 and Ev6 occurred after the deposition of unit S52 and during unit S51 deposition. During this period, reverse and normal subsidiary fault displacements are observed in W4-W8 even after restoring the fault displacement of Ev2 to Ev4 (Fig. 7). Although it is possible that both displacements occurred during a single event, we estimate two separate events (Ev5 and Ev6). From the retrodeformation (Figs. 7 and S2), we found that the displacement patterns tended to be similar in consecutive events. In other words, Ev0 and Ev1 created open cracks along the primary normal fault (W8-W9), and Ev2 to Ev4 caused reverse fault displacement in the southern part and normal fault displacement on the primary normal fault. Additionally, Ev7 involves only normal fault displacement as described in the following paragraph. Considering the similarity of the displacement patterns in consecutive events, reverse fault motions could be related to Ev5, and normal fault motion could be related to Ev6 (Fig. 7). Therefore, we interpreted that there could have been two events during this period; however, we recognize that the observed deformation can also be attributed to a single event. Since the ages of Ev5 and Ev6 cannot be distinguished, both events are only constrained as after unit S52 and during unit S51 deposition.

In Ev7, a normal fault displacement at W7-W8 occurred at the lowest part of the soil deposits in this trench. On the west wall, even after restoring the fault displacement of Ev2 to Ev6, vertical displacement was still observed in the normal fault at W6 (Fig. 7) from which we infer the occurrence of Ev7. Its age is estimated to be between units S52 and S53 deposition. We recognize that the small amount of remaining offset after retrodeformation could be related to thickness (facies) changes in the deposit, variable deformation related to the later events, and/or a component of oblique slip and not necessarily require an additional earthquake. Units 60-64 may represent sediments downdropped in earlier events; however, the available exposure is complicated and precludes clear identification of additional events. Thus, an unknown number of events may have occurred prior to about 15 ka. Deeper excavations would be required to test this possibility.

5 Discussion

5.1 Slip partition based on 3D displacements

In this section, we discuss how the displacement is divided on the Futagawa and Idenokuchi faults for the slip partition along line A (Fig. 5), where the influence of surface failure is small and the Futagawa fault appeared as a single trace (Fig. 4). First, dextral displacement occurred only on the Futagawa fault. Local sinistral displacement was observed along the Idenokuchi fault in the field (Toda et al., 2016; Shirahama et al., 2016). However, the amount of lateral displacement remained consistent across the Idenokuchi fault over a long distance (> 3 km) along Line A. On the other hand, the vertical displacement is the opposite of the lateral displacement. Vertical displacement of 1 m occurred only in the southernmost trace of the Idenokuchi fault along the long survey line, and little vertical displacement occurred within a 1 km width across the Futagawa fault. Vertical displacement of several tens of centimeters occurred on the subparallel faults of the Idenokuchi fault, but that decreased immediately within a short distance from the fault, indicating that the deformation was localized to a shallow depth. These observations suggest that extensional deformation and block rotation cause apparent vertical displacement on the subparallel faults.

Scott et al. (2018) and Himematsu and Furuya (2020) observed a large vertical displacement (1-2 m south-up) on the Futagawa fault on the west side of the parallel section of the Futagawa and Idenokuchi faults. This indicates that the Futagawa fault accommodated oblique slip on the west side of the Idenokuchi fault's parallel section. In addition, Himematsu and Furuya (2020) showed a sharp decrease in vertical displacement and nearly constant right lateral displacement along the Futagawa fault at the parallel section of the Idenokuchi fault, which is consistent with our results.

Our observations suggest that the slip partition on the Futagawa and Idenokuchi faults is the result of oblique lateral displacement at depth, which is almost completely split into dextral and vertical displacement near the surface and accommodated by both faults, respectively, as shown schematically by Toda et al. (2016). In addition, our results show that the displacement is completely split, as shown in King et al. (2005). This may provide an important insight into the geometry (dip angle, distance of two faults, and amount of oblique displacement) of faults where slip partitioning can occur. We interpret that the deeper part of the Idenokuchi fault is connected to the deeper part of the Futagawa fault, and the Idenokuchi fault is a branch fault of the Futagawa fault. The estimated depth at which they merge may be several kilometers, as shown by Toda et al. (2016), although it depends on their dip angles (the dip of the Idenokuchi fault was estimated to 50°–70° north).

We discuss the relationship between slip partition and geology. According to King et al. (2005), the depth at which the fault branches upwards may coincide with the bottom of surface sediments. Aoyagi et al. (2024) reported another slip partition on the western part of the Futagawa fault based on the surface rupture distribution of the 2016 event, drilling cores, and seismic reflection survey. They reported that the short (<2 km) subparallel surface ruptures/faults accommodated oblique slip in the deeper part of the 2016 Kumamoto earthquake and converged at a depth of 350 m. The depth corresponds to the top of the pre-Aso volcanic rocks and/or Kiyama metamorphic rocks (Kumamoto Prefecture Geological Map Compilation Committee, 2008). Unconsolidated sediments, including pyroclastic flow deposits of middle to late Pleistocene age, overlie these rocks. Thus, the upper end depth (convergent depth of both faults) of oblique slip seems to correspond to some geological (physical property) difference. There is no data

on the deep subsurface geology of our study area. Since there is no surface sediment (unconsolidated) and pre-Aso volcanic rocks are exposed on the surface around the trench site, the situation differs from that in King et al. (2005) and Aoyagi et al. (2024).

5.2 Age of paleofaulting events on the Idenokuchi fault

Based on evidence for paleofaulting events, we infer six certain faulting events including Ev0–Ev4 and a single event (combined Ev5/Ev6) that occurred since the deposition unit S53. We also interpret several additional less certain events including Ev7 and the possibility that two events occurred after the deposition of S52 (Ev5 and Ev6 as separate events). The ages of the faulting events were obtained using OxCal (Fig. S4). The results show that the ages of each event are as follows: Ev1: 2190–940 cal BP, Ev2: 4760–4250 cal BP, Ev3: 6040–5360 cal BP, Ev4: 9550–7280 cal BP, Ev5-Ev6: 13500–9680 cal BP, Ev7: 14700–13840 cal BP with the 2σ range. The average recurrence interval of the maximum of eight interpreted events is 1990–2110 years, while the average recurrence interval for six certain events was 2780–2950 years.

Unit S53 is buried 4.5–5 m below the present ground surface, indicating that the strata dropped an average of 0.6–0.8 m per event (six to eight events) relative to the ground surface. This value is roughly consistent with a representative 2016 coseismic displacement of 60 cm along the surface rupture, where the KMR trench was excavated. Despite the shallow depth of the trench, we could identify up to eight events, significantly more than those identified in trenches excavated on the primary Futagawa fault. Along the Futagawa fault, large single-event displacements and intense cumulative deformation often complicate the restoration of individual events on trench walls. Furthermore, strike-slip components can limit the reliability of event chronologies within a single trench. For instance, at the Futa site on the Futagawa fault (Fig. 1; Ishimura et al., 2022), although multiple trenches were excavated across both strike-slip and subsidiary normal faults, the number of identifiable events from the strike-slip faults remained limited. In contrast, at our study site, the predominantly dip-slip (vertical) movement and smaller displacement per event allowed for a more detailed identification of past faulting events, even within a shallow depth. This result underscores the importance of targeting sites with small per-event displacements, alongside regional advantages such as relatively rapid and continuous sedimentation.

5.3 Comparison of paleoseismic events between the Futagawa and other faults

A summary of the paleofaulting history shows that the ages of faulting events after the K-Ah tephra (7.3 ka), which is widely identified in the paleoseismic trenches around the Futagawa fault, all overlap (Fig. 8). This suggests that, at least for the past several earthquakes. The Futagawa fault (Ishimura et al., 2022), Miyaji faults (Ishimura et al., 2021), and Idenokuchi fault have all moved simultaneously, similar to the 2016 event. Notably, the simultaneity of the Futagawa and Idenokuchi faults is consistent with the idea that they are connected at a deeper level, as described in Section 5.1. Therefore, the paleoseismic history of the Idenokuchi fault may suggest a close relationship with that of the Futagawa fault, given its subsurface structure. The Miyaji faults, which produced the 2016 surface rupture and are distant from the Futagawa fault and structurally discontinuous (Fukushima and Ishimura, 2020), are also presumed to have been active in the past, together with the Futagawa fault. Given inherent uncertainties in dating techniques, it is technically challenging to prove the simultaneous rupture of faults. Nevertheless, further studies are necessary to determine whether the simultaneous rupture of the primary and secondary faults is common or if it is worthwhile to incorporate small displacements relative to those on the primary fault into seismic hazard assessment.

Furthermore, assuming that the faulting events from Ev1 to Ev3 are the same among our three trenches (Komori, Miyaji, and Futa trenches), the calculated ages in OxCal modeling are Ev1: 2060–1760 cal BP, Ev2: 4420–4180 cal BP, and Ev3: 6000–5370 cal BP (Fig. 8). The recurrence intervals of each event are Ev0/Ev1: 1830–2120 years, Ev1/Ev2: 2210–2590 years, and Ev2/Ev3: 1040–1720 years with the 2σ range. Based on the trenching results, the average recurrence interval from Ev0 to Ev7 is 1990–2110 years, consistent with the modeled recurrence interval from Ev0 to Ev3. This potentially indicates that the Futagawa fault has ruptured with a degree of periodicity.

The dextral slip rate, calculated from the recurrence interval (1990–2110 years) and single displacement (1.8–3.1 m) obtained in this study, is 0.9–1.5 mm/yr for the Futagawa fault. For the Idenokuchi fault, the vertical displacement ranges from 1.0 to 2.5 m, indicating an estimated vertical slip rate of 0.5 to 1.3 mm/yr. West of the study area (Futa to Ohkirihata), Ishimura (2019) calculated a vertical slip rate (0.9–1.1 mm/yr) and a dextral slip rate (1.5–3.7 mm/yr) for the Futagawa fault from the vertical and dextral displacements of Takayubaru lava (K–Ar ages 81 ± 4 ka and 98 ± 18 ka; Miyoshi et al., 2013). The Idenokuchi fault runs parallel to the Futagawa fault, where these slip rates, i.e., the west of the study area, were calculated. However, the vertical displacement on the Idenokuchi fault in the 2016 event west of the study area is small (Kaneda et al., 2022). Therefore, the long-term slip rates can be regarded as representative values when oblique slip is accommodated only by the Futagawa fault. Therefore, the long-term dextral and vertical slip rates are consistent with the results of this study. Oohashi et al. (2020) pointed out that normal fault displacement was predominant on the Futagawa fault before Aso-4 pyroclastic flow deposits (87 ka; Aoki, 2008), and dextral displacement became apparent later. Oohashi et al. (2020) proposed the following possibilities for this change: 1) The stress field changed from a normal fault type with north-south extension to a dextral strike-slip fault type with predominant east-west compression, and 2) the normal fault component of the Futagawa fault was replaced by the

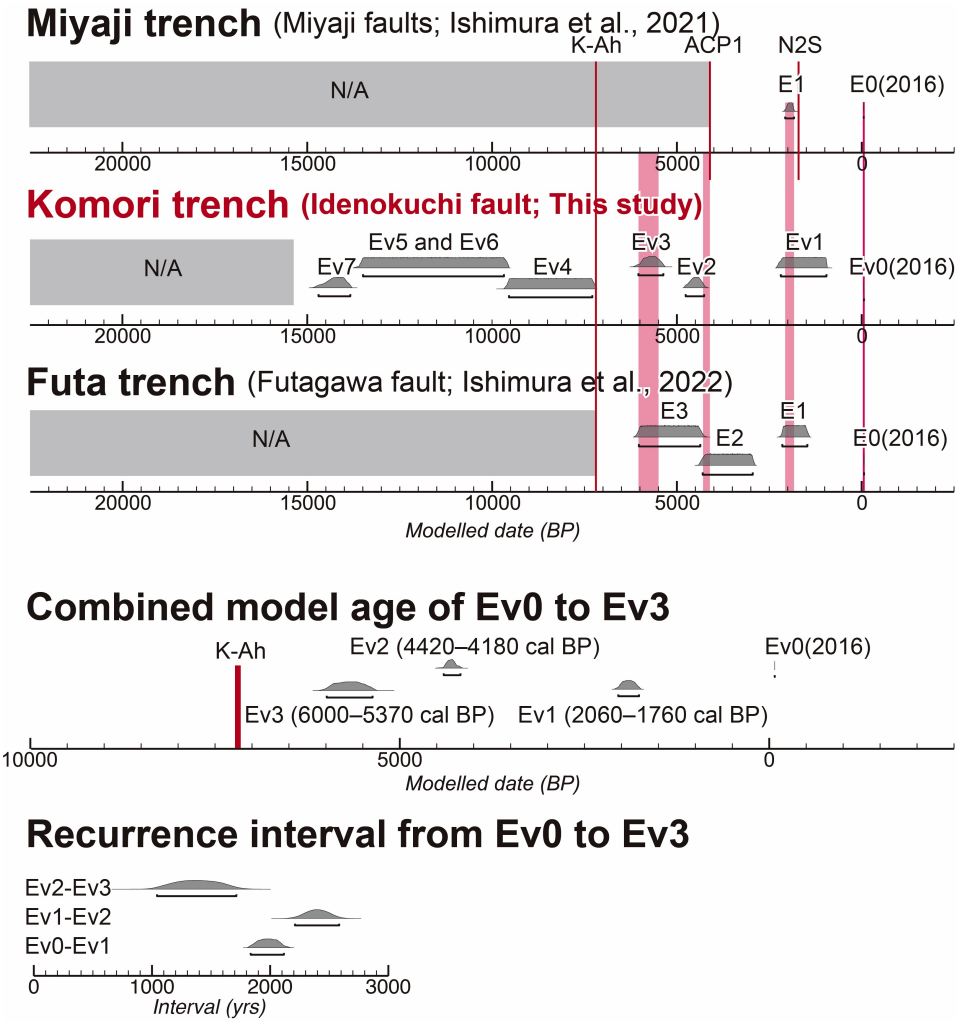

Figure 8 Modeled event ages and comparison to the authors' previous paleoseismic studies. The underbars show the 2σ probability distribution ranges of the modeled ages. ACP1 and N2S are local tephras from the Aso volcano (Table S1; Miyabuchi, 2009). ACP1 is Aso central cone pumice and its age is 4.1 ka (Miyabuchi, 2009). N2S is Nakadake N2 scoria, and its age is 1490–1470 cal BP (68.2%) (Yamada et al., 2017).

Idenokuchi fault and off-fault displacements, and the dextral displacement of the Futagawa fault became apparent. The fact that the long-term vertical slip rate coincides with that of the Idenokuchi fault from this study agrees with the second explanation. Therefore, the slip partition on the Idenokuchi fault must have commenced after the Aso-4 event (ca. 87 ka).

Figure 9 summarizes the paleofaulting history of the Kumamoto earthquake area since 7.3 ka, based on previous paleoseismic results, including archaeological information. The number of earthquakes since 7.3 ka (including 2016) on the Futagawa fault is estimated to be four with considerable accuracy and precision, based on the results of multiple trenches along the Futagawa fault and its vicinity. Accurate ages for the past three events are available from this and previous studies by our group, which targeted sites with minimal artificial disturbance, continuous sedimentary records, and well-defined tephra layers to ensure high-resolution chronologies. In addition, the paleofaulting history at the northwestern Aso caldera (Sato et al., 2021) and the western part of the Futagawa fault (Inoue et al., 2020), which are at secondary surface ruptures, indicates that one of their events coincides with Ev1 in this study. Therefore, it is highly likely that the secondary faults were activated simultaneously during at least the penultimate event of the Futagawa fault. Lateral spreading recognized at archaeological sites within the caldera (Kumamoto Prefectural Board of Education, 2010; Aso City Board of Education, 2011) was also approximately 2000 years ago, which also supports that secondary phenomena caused by an earthquake similar to the 2016 event occurred repeatedly in the caldera. Thus, it is inferred that similar phenomena in the 2016 event (e.g., secondary surface rupture, liquefaction, and lateral spreading) also occurred during the previous activity. However, the age of the antepenultimate event in the northwestern part of the caldera does not match that of the Futagawa fault (Sato et al., 2021). In addition, no other secondary surface ruptures have been identified as having earthquakes older than the antepenultimate event, so it is unclear how the secondary fault behaved during the older events. Future information on the presence or absence of older earthquakes on such secondary faults and their histories will help us to better understand the secondary faults and how frequently

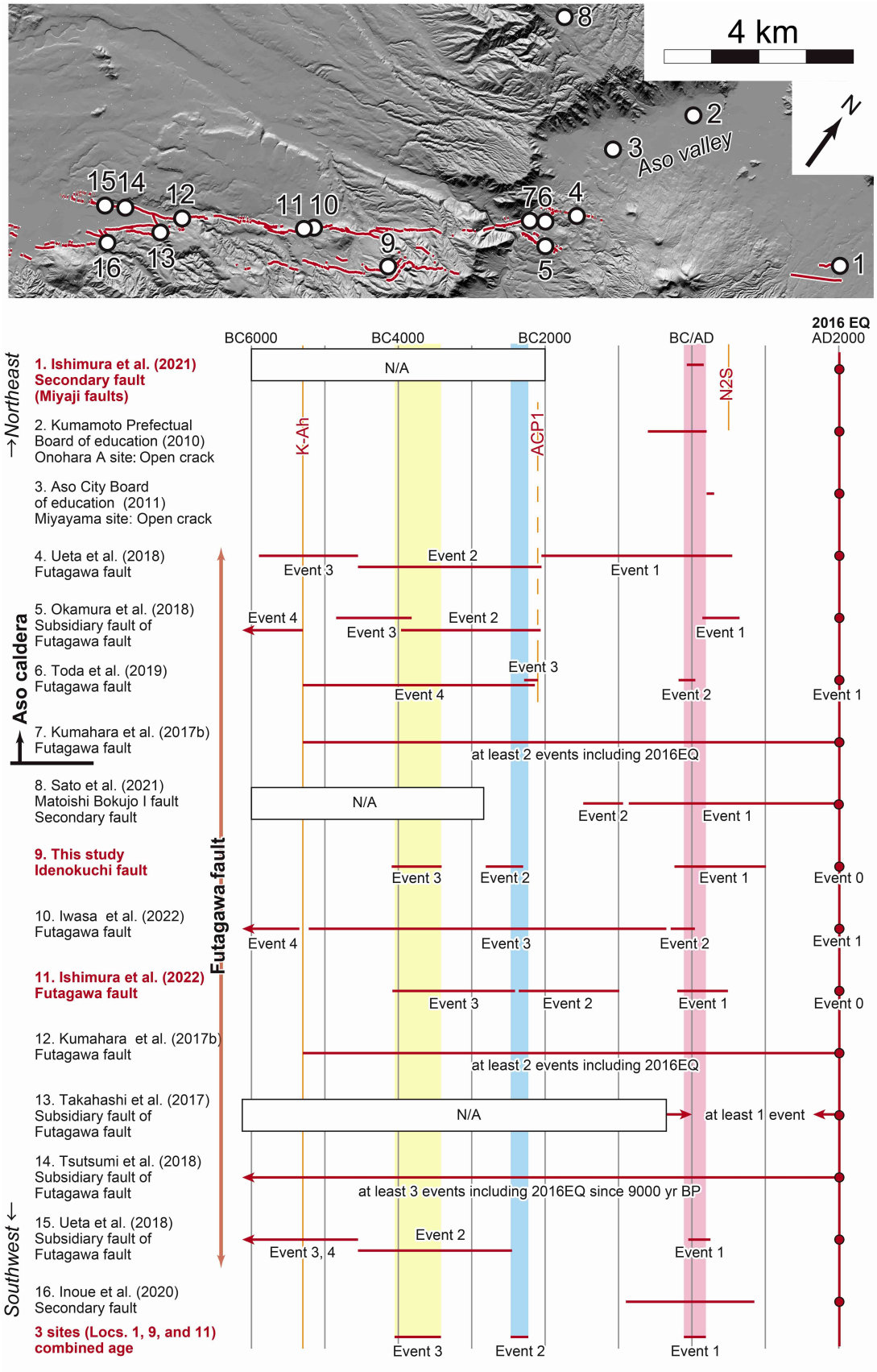

Figure 9 Compilation of paleofaulting events. The upper panel shows the locations of the lower panel data. The lower panel shows the compiled spatial-temporal age distribution of the paleofaulting events along the Futagawa and its subsidiary and secondary faults. Event chronologies correspond to studies referenced on the left side of the panel. The red bar represents the event age range in each study. The red arrow indicates that the age is estimated to be outside the range shown in the figure. The pink, blue, and yellow shading represent the combined model age ranges of Ev1, Ev2, and Ev3, respectively. Details of ACP1 and N2S tephras were described in the caption of Figure 8.

they rupture simultaneously with the Futagawa fault.

6 Conclusions

Using the 2016 Kumamoto earthquake as an example, we performed a DTM difference analysis in the area where the Futagawa and Idenokuchi faults interact, and conducted an excavation survey on the Idenokuchi fault. Based on the 3D displacement distribution, we discussed how the slip partition occurred on them and found that the oblique slip at depth was split entirely into vertical and horizontal displacements on the ground surface. This indicates that the Idenokuchi fault is structurally related to the Futagawa fault and that the paleofaulting history of the Idenokuchi fault may correspond to that of the Futagawa fault.

The KMR trench at the Idenokuchi fault revealed continuous deposition of soil and tephra since 15 ka, and retrodeformation of the trench walls revealed at least six and up to eight faulting events (including 2016) during this period. Among them, the faulting events after Kikai-Akahoya tephra (7.3 ka) are consistent with paleoseismic surveys on the Futagawa fault (the primary fault) and Miyaji faults (secondary faults in the Aso caldera). This suggests that at least some surface ruptures that occurred around the Futagawa fault during the 2016 event were likely active at the same time as past activities of the Futagawa fault. The activity histories since 7.3 ka with the authors' three trenches on the Futagawa, Miyaji, and Idenokuchi faults are E1: 2060–1760 cal BP, E2: 4420–4180 cal BP, and E3: 6000–5370 cal BP, indicating that they occurred relatively periodically. The mean recurrence interval since 15 ka is about 2000-3000 years, supporting the periodic activity. The results of this study are also consistent with other trench investigations conducted after 2016. It is important to improve the accuracy and precision of the activity history of the Futagawa fault before 7.3 ka and to investigate the activity history of the Hinagu fault zone in the southern part of the Futagawa fault zone to consider future seismic hazard and interlocking rupture. In addition, it will be important to clarify the subsurface structure and activity history of secondary faults in other earthquakes to consider displacement hazards.

Acknowledgements

We thank Yasuhiro Kumahara, Ryuhei Oda, Jun Matsukaze, Motoya Kobayashi, Makoto Kobayashi, Yoshiya Iwasa, and Daichi Tomita for their help during the trench survey. We also thank Shinji Toda, Heitaro Kaneda, and Yasuo Miyabuchi for their discussions and constructive comments. The thoughtful comments from the reviewer Rich Koehler, the anonymous reviewer, and the editor Randolph Williams improved the article. This work was supported by KAKENHI Grant Number JP17H04730 from the Japan Society for the Promotion of Science.

Data and code availability

Supplementary figures (S1 to S2) and tables (S1 to S5) are available in the supplement material. OxCal model codes are listed in the supplementary material. Pre- and post-event DTMs used in this study were provided by the Geospatial Information Authority of Japan (https://www.gsi.go.jp/ENGLISH/index.html).

Competing interests

The authors have no competing interests.

References

Aoki, K. Revised age and distribution of ca. 87 ka Aso-4 tephra based on new evidence from the northwest Pacific Ocean. *Quaternary International*, 178(1):100–118, 2008.

Aoyagi, Y., Higashi, S., Homma, S., S., M., Sugiyama, M., and Hijikata, K. Surface ruptures in the Aso campus of Tokai University caused by the 2016 Kumamoto Earthquake. *Active Fault Research*, (55):1–18, 2021.

Aoyagi, Y., Ueta, K., Takemoto, T., Suehiro, M., and Miyawaki, R. Seismic constraints on the subsurface extent of subparallel surface ruptures in Mashiki Town, Japan, associated with the 2016 Kumamoto Earthquake. *Journal of the Seismological Soceity of Japan*, 2nd ser.(77):5–19, 2024.

Aso City Board of Education. Miyayama ruins II. *Cultural Property Investigation Report of Aso City 2*, 2011.

Barnhart, W. D., Hayes, G. P., and Gold, R. D. The July 2019 Ridgecrest, California, earthquake sequence: Kinematics of slip and stressing in cross-fault ruptures. *Geophysical Research Letters*, 46(21):11859–11867, 2019.

Danhara, T., Yamashita, T., Iwano, H., and Kasuya, M. An improved system for measuring refractive index using the thermal immersion method. *Quaternary International*, 13:89–91, 1992.

Fujiwara, S., Yarai, H., Kobayashi, T., Morishita, Y., Nakano, T., Miyahara, B., Nakai, H., Miura, Y., Ueshiba, H., Kakiage, Y., et al. Small-displacement linear surface ruptures of the 2016 Kumamoto earthquake sequence detected by ALOS-2 SAR interferometry. *Earth, Planets and Space*, 68(1):160, 2016.

Fukushima, Y. and Ishimura, D. Characteristics of secondary-ruptured faults in the Aso Caldera triggered by the 2016 Mw 7.0 Kumamoto earthquake. *Earth, Planets and Space*, 72(1):175, 2020.

Goto, H., Tsutsumi, H., Toda, S., and Kumahara, Y. Geomorphic features of surface ruptures associated with the 2016 Kumamoto earthquake in and around the downtown of Kumamoto City, and implications on triggered slip along active faults. *Earth, Planets and Space*, 69(1):1–12, 2017.

Hamling, I. J., Hreinsdóttir, S., Clark, K., Elliott, J., Liang, C., Fielding, E., Litchfield, N., Villamor, P., Wallace, L., Wright, T. J., et al. Complex multifault rupture during the 2016 M w 7.8 Kaikōura earthquake, New Zealand. *Science*, 356(6334):eaam7194, 2017.

He, P., Wen, Y., Xu, C., and Chen, Y. Complete three-dimensional near-field surface displacements from imaging geodesy techniques applied to the 2016 Kumamoto earthquake. *Remote Sensing of Environment*, 232:111321, 2019.

Headquarters for Earthquake Research Promotion. Long-term evaluation of the Futagawa and Hinagu fault zones. 2013. http://www.jishin.go.jp/main/chousa/13feb_chi_kyushu/k_11.pdf.

Himematsu, Y. and Furuya, M. Coseismic and postseismic crustal deformation associated with the 2016 Kumamoto earth-

quake sequence revealed by PALSAR-2 pixel tracking and InSAR. *Earth and Space Science*, 7(10):e2020EA001200, 2020. doi: 10.1029/2020EA001200.

Hoshizumi, H., Ozaki, M., Miyazaki, K., Matsuura, H., Toshimitsu, S., Uto, K., Uchiumi, S., Komazawa, M., Hiroshima, T., and Sudo, S. Geological Map of Japan 1:200,000, Kumamoto. *Geological Society of Japan, AIST*, 2004.

Inoue, N., Kitada, N., Shibuya, N., Omata, M., Takahama, T., Tonagi, M., and Irikura, K. Probabilistic evaluation of off-fault displacements of the 2016 Kumamoto earthquake. *Pure and Applied Geophysics*, 177(5):2007–2019, 2020. doi: 10.1007/s00024-019-02345-7.

Ishimura, D. Coseismic vertical displacement associated with the 2016 Kumamoto earthquake (Mw7.0) and activity of the Futagawa fault around Futa, Nishihara Village, Kumamoto prefecture. *Active Fault Resarch*, (50):33–32, 2019.

Ishimura, D. and Kakiuchi, Y. Chronology and processes of fluvial terrace formation in northeastern Kinki district, southwest Japan, based on cryptotephra analysis. *Quaternary International*, 246(1-2):190–202, 2011.

Ishimura, D., Toda, S., Ichihara, T., Takahashi, N., Konno, A., and Sato, H. A study on surface ruptures around Miyaji, Aso City, Kumamoto Prefecture, associated with the 2016 Kumamoto earthquake sequence and upward slip tapering on pit excavation walls. *Active Fault Research*, (47):9–16, 2017.

Ishimura, D., Toda, S., Mukoyama, S., Homma, S., Yamaguchi, K., and Takahashi, N. 3D Surface displacement and surface ruptures associated with the 2014 M w 6.2 Nagano earthquake using differential lidar. *Bulletin of the Seismological Society of America*, 109(2):780–796, 2019. doi: 10.1785/0120180020.

Ishimura, D., Tsutsumi, H., Toda, S., Fukushima, Y., Kumahara, Y., Takahashi, N., Ichihara, T., and Takada, K. Repeated triggered ruptures on a distributed secondary fault system: an example from the 2016 Kumamoto earthquake, southwest Japan. *Earth, Planets and Space*, 73(1):1–17, 2021. doi: 10.1186/s40623-021-01371-x.

Ishimura, D., Iwasa, Y., Takahashi, N., Tadokoro, R., and Oda, R. Paleoseismic events and shallow subsurface structure of the central part of the Futagawa fault, which generated the 2016 Mw 7.0 Kumamoto earthquake. *Geomorphology*, 414:108387, 2022. doi: 10.1016/j.geomorph.2022.108387.

Iwasa, Y., Kumahara, Y., Goto, H., Ishimura, D., and Hosoya, T. Faulting history of the Futagawa fault zone based on trenching survey at Komori, Nishihara Village, Kumamoto Prefecture. *Active Fault Research*, (56):47–58, 2022.

Kamata, H. and Kodama, K. Tectonics of an arc-arc junction: an example from Kyushu Island at the junction of the Southwest Japan Arc and the Ryukyu Arc. *Tectonophysics*, 233(1-2):69–81, 1994. doi: 10.1016/0040-1951(94)90220-8.

Kaneda, H. and Chiba, T. Stereopaired morphometric protection index red relief image maps (Stereo MPI-RRIMs): effective visualization of high-resolution digital elevation models for interpreting and mapping small tectonic geomorphic features. *Bulletin of the Seismological Society of America*, 109(1):99–109, 2019. doi: 10.1785/0120180166.

Kaneda, H., Toda, S., Ishimura, D., Kumahara, Y., Goto, H., Okada, S., and Kobayashi, M. Surface Ruptures and Tectonic Geomorphology Along and Around the Idenokuchi Fault. In *Surface Ruptures Associated with the 2016 Kumamoto Earthquake Sequence in Southwest Japan*, pages 151–179. Springer, 2022. doi: 10.1007/978-981-19-1150-7$_1$2.

King, G., Klinger, Y., Bowman, D., and Tapponnier, P. Slip-partitioned surface breaks for the M w 7.8 2001 Kokoxili earthquake, China. *Bulletin of the Seismological Society of America*, 95(2):731–738, 2005. doi: 10.1785/0120040101.

Kokusai Kogyo Co., Ltd. 3D-Geomorphic Image Velocimetry, JP Patent No. 4545219, 2010.

Kumahara, Y., Okada, S., Kagohara, K., Kaneda, H., Goto, H., and Tsutsumi, H. 1:25,000 Active Fault Map, Futagawa-Hinagu Fault Zone and its Vicinity "Kumamoto (Revision)". *Geospatial Information Authority of Japan, Ibaraki*, 2017a.

Kumahara, Y., Torii, M., Nakata, T., et al. Fault history of the northern part of Futagawa-Hinagu fault zone based on trench survey at Dozon. In *Mashiki Town and at Kawayo, Minami-Aso Village, Programme and abstracts JSAF 2017 fall meeting, Hiroshima University, Higashi-Hiroshima*, pages 24–25, 2017b.

Kumahara, Y., Kaneda, H., and Tsutsumi, H. Surface ruptures associated with the 2016 Kumamoto earthquake sequence in southwest Japan. In *Advances in Geological Science*. Springer Nature, 2022. doi: 10.1007/978-981-19-1150-7.

Kumamoto Prefectural Board of Education. Earthquake traces in Onobaru-A site. Onobaru ruins group. In *Cultural Property Investigation Report of Kumamoto Prefecture*, volume 257, pages 147–149. 2010.

Kumamoto Prefecture Geological Map Compilation Committee. Geological Map of the Kumamoto Prefecture (1:100,000). 2008.

Litchfield, N. J., Villamor, P., Dissen, R. J. V., Nicol, A., Barnes, P. M., A. Barrell, D. J., Pettinga, J. R., Langridge, R. M., Little, T. A., Mountjoy, J. J., et al. Surface rupture of multiple crustal faults in the 2016 M w 7.8 Kaikōura, New Zealand, Earthquake. *Bulletin of the Seismological Society of America*, 108(3B):1496–1520, 2018. doi: 10.1785/0120170300.

Machida, H. and Arai, F. *Atlas of Tephra in and around Japan [revised edition]*. University of Tokyo Press, Tokyo, 2003.

Matsumoto, Y. Some problems on volcanic activities and depression structures in Kyushu, Japan. *Memoirs of the Geological Society of Japan*, 16:127–139, 1997.

Miyabuchi, Y. A 90,000-year tephrostratigraphic framework of Aso Volcano, Japan. *Sedimentary Geology*, 220(3-4):169–189, 2009. doi: 10.1016/j.sedgeo.2009.04.018.

Miyoshi, M., Shinmura, T., Sumino, H., Sano, T., Miyabuchi, Y., Mori, Y., Inakura, H., Furukawa, K., Uno, K., Hasenaka, T., et al. Lateral magma intrusion from a caldera-forming magma chamber: Constraints from geochronology and geochemistry of volcanic products from lateral cones around the Aso caldera, SW Japan. *Chemical Geology*, 352:202–210, 2013. doi: 10.1016/j.chemgeo.2013.06.003.

Moya, L., Yamazaki, F., Liu, W., and Chiba, T. Calculation of coseismic displacement from lidar data in the 2016 Kumamoto, Japan, earthquake. *Natural Hazards and Earth System Sciences*, 17(1):143–156, 2017. doi: 10.5194/nhess-17-143-2017.

Mukoyama, S. Estimation of ground deformation caused by the earthquake (M7. 2) in Japan, 2008, from the geomorphic image analysis of high resolution LiDAR DEMs. *Journal of Mountain Science*, 8(2):239–245, 2011. doi: 10.1007/s11629-011-2106-7.

Muroi, S., Suzuki, Y., Mukoyama, S., Iwasa, Y., Yamashita, H., Muraki, M., Yamashita, K., and Fukuba, T. Surface displacement vector discontinuity in the easternmost part of the Futagawa-Hinagu fault zone analyzed by using airborne laser scanning data at two different timings. *Active Fault Research*, (60):11–25, 2024.

Nakata, T. and Imaizumi, T. *Digital Active Fault Map of Japan*. University of Tokyo Press, Tokyo, 2002.

Nurminen, F., Boncio, P., Visini, F., Pace, B., Valentini, A., Baize, S., and Scotti, O. Probability of occurrence and displacement regression of distributed surface rupturing for reverse earthquakes. *Frontiers in Earth Science*, 8:581605, 2020. doi:

10.3389/feart.2020.581605.

Nurminen, F., Baize, S., Boncio, P., Blumetti, A. M., Cinti, F. R., Civico, R., and Guerrieri, L. SURE 2.0–New release of the world-wide database of surface ruptures for fault displacement hazard analyses. *Scientific Data*, 9(1):729, 2022. doi: 10.1038/s41597-022-01835-z.

Okamura, Y., Abe, S., Miyashita, Y., Azuma, T., Togo, T., Shirahama, Y., Awata, Y., Maruyama, T., Ogami, T., Imura, R., Tsutsumi, H., Goto, H., and Kumahara, Y. 3.1 Survey of detailed position and shape of active faults to understand the fault segments and observation to reveal the paleoseismic history and slip rates. In *Research Report of a Comprehensive Active Fault Survey After the 2016 Kumamoto Earthquake, 2017 Fiscal Year*. Ministry of Education, Culture, Sports, Science and Technology and Kyushu University, 2018.

Oohashi, K., Otsubo, M., Matsumoto, S., Kobayashi, K., Sato, K., and Nishimura, T. The Quaternary tectonics of central Kyushu and the 2016 Kumamoto earthquake: From a multifaceted viewpoint combining geology, seismology, and geodesy. *Journal of Geography (Chigaku Zasshi)*, 129:565–589, 2020.

Ramsey, C. B. Deposition models for chronological records. *Quaternary Science Reviews*, 27(1-2):42–60, 2008.

Reimer, P. J., Austin, W. E., Bard, E., Bayliss, A., Blackwell, P. G., Ramsey, C. B., Butzin, M., Cheng, H., Edwards, R. L., Friedrich, M., et al. The IntCal20 Northern Hemisphere radiocarbon age calibration curve (0–55 cal kBP). *Radiocarbon*, 62(4):725–757, 2020. doi: 10.1017/RDC.2020.41.

Research Group for Active Faults of Japan. *Active Faults in japan, Sheet Maps and Inventories*. University of Tokyo Press, Tokyo, 1980.

Research Group for Active Faults of Japan. *Active Faults in Japan, Sheet Maps and Inventories, Rev. Ed.* University of Tokyo Press, Tokyo, 1991.

Sato, H., Komura, K., Une, H., Nakano, T., and Yagi, H. Study on cumulative activities of passively ruptured faults through a trenching survey at the Matoishi Bokujo I Fault, northwest side of the Aso caldera, southwestern Japan. *Geogr Rev Jpn Ser A*, 94(4): 250–264, 2021. doi: 10.4157/grj.94.250.

Scott, C. P., Arrowsmith, J. R., Nissen, E., Lajoie, L., Maruyama, T., and Chiba, T. The M7 2016 Kumamoto, Japan, earthquake: 3-D deformation along the fault and within the damage zone constrained from differential lidar topography. *Journal of Geophysical Research: Solid Earth*, 123(7):6138–6155, 2018. doi: 10.1029/2018JB015581.

Seno, T., Stein, S., and Gripp, A. E. A model for the motion of the Philippine Sea plate consistent with NUVEL-1 and geological data. *Journal of Geophysical Research: Solid Earth*, 98(B10): 17941–17948, 1993. doi: 10.1029/93JB00782.

Shirahama, Y., Yoshimi, M., Awata, Y., Maruyama, T., Azuma, T., Miyashita, Y., Mori, H., Imanishi, K., Takeda, N., Ochi, T., Otsubo, M., Asahina, D., and Miyakawa, A. Characteristics of the surface ruptures associated with the 2016 Kumamoto earthquake sequence, Central Kyushu, Japan. *Earth, Planets, and Space*, 68 (191), 2016. doi: 10.1186/s40623-016-0559-1.

Shirahama, Y., Miyashita, Y., Kametaka, M., Suzuki, Y., Miyairi, Y., and Yokoyama, Y. Detailed paleoseismic history of the Hinagu fault zone revealed by the high-density radiocarbon dating and trenching survey across a surface rupture of the 2016 Kumamoto earthquake, Kyushu, Japan. *Island Arc*, (30):e12376, 2021. doi: 10.1111./iar.12376.

Smith, V., Staff, R., Blockley, S., Bronk Ramsey, C., Nakagawa, T., Mark, D., Takemura, K., and Danhara, T. Identification and correlation of visible tephras in the Lake Suigetsu SG06 sedimentary archive, Japan: chronostratigraphic markers for synchronising of east Asian/west Pacific palaeoclimatic records across the last 150 ka. *Quaternary Science Reviews*, (67):121–137, 2013. doi: 10.1016/j.quascirev.2013.01.026.

Suzuki, T., Kasahara, A., Nishizawa, F., and Saito, H. Chemical characterization of volcanic glass shards by energy dispersive X-ray spectrometry with EDAX Genesis APEX2 and JEOL JSM-6390. *Geographical reports of Tokyo Metropolitan University*, (49):1–12, 2014.

Suzuki, Y., Ishimura, D., Kumaki, Y., Kumahara, Y., Chida, N., Nakata, T., and Nakano, T. *1:25,000 Active Fault Map, Futagawa-Hinagu Fault Zone and its Vicinity "Aso"*. Geospatial Information Authority of Japan, Ibaraki, 2017.

Takahashi, N., Ishimura, D., Toda, S., Nakata, T., and Watanabe, M. Vertical slip rate on a normal fault co-ruptured with the Futagawa fault at the 2016 Kumamoto earthquake. *Active Fault Research*, (46):27–32, 2017.

Toda, S., Kaneda, H., Okada, S., Ishimura, D., and Mildon, Z. Slip-partitioned surface ruptures for the Mw 7.0 16 April 2016 Kumamoto, Japan, earthquake. *Earth, Planets, and Space*, (68): 188, 2016. doi: 10.1186/s40623-016-0560-8.

Toda, S., Torii, M., Okuno, M., Konno, A., Ono, H., and Takahashi, N. Evidence for Holocene paleoseismic events on the 2016 Kumamoto earthquake rupture zone within the Aso caldera: a trench excavation survey at Kurokawa, the town of Minami-Aso, Southwest Japan. *Active Fault Research*, (51):13–25, 2019.

Tsutsumi, H., Toda, S., Goto, H., Kumahara, Y., Ishimura, D., Takahashi, N., Taniguchi, K., Omata, M., Kohriya, Y., Gomi, M., Asano, K., and Iwata, T. Paleoseismic trenching across the surface rupture of the 2016 Kumamoto earthquake at Jichu, Mashiki Town, Kumamoto Prefecture. *Active Fault Research*, (49):31–39, 2018.

Ueta, K., Miyawaki, R., Iemura, K., Yokoyama, T., and Miyawaki, A. Paleoseismological study on surface fault ruptures produced by the 2016 Kumamoto earthquake. In *Abstracts of Japan Geoscience Union Meeting 2018, Makuhari Messe, Chiba*, 2018.

Watanabe, K. and Ono, K. Geology of the vicinity of Omine on the western flank of the Aso caldera. *Journal of the Geological Society of Japan*, (75):365–374, 1969.

Xu, X., Sandwell, D., and Smith-Konter, B. Coseismic Displacements and Surface Fractures from Sentinel-1 InSAR: 2019 Ridgecrest Earthquakes. *Seismological Research Letters*, (91): 1979–1985, 2020. doi: 10.1785/0220190275.

Yamada, K., Takemura, K., Kuwae, M., Yamamoto, M., and Danhara, T. Revised ages of late Holocene tephras in Beppu Bay, central Kyushu, southwest Japan. *Quaternary International*, (452): 33–42, 2017. doi: 10.1016/j.quaint.2017.01.024.